ISSN 2812-9474

Engineering TODAY

VOL. 1 / NO. 3 / 2022

PUBLISHED BY

The Faculty of Mechanical and Civil Engineering
in Kraljevo of the University of Kragujevac

ISSN 2812-9474

VOL. 1 / NO. 3 / 2022

ET Engineering TODAY

PUBLISHED BY

The Faculty of Mechanical and Civil Engineering
in Kraljevo of the University of Kragujevac

Engineering TODAY

PUBLISHER

The Faculty of Mechanical and Civil Engineering in Kraljevo of the University of Kragujevac

ADDRESS

Faculty of Mechanical and Civil Engineering

Dositejeva 19, 36000 Kraljevo
Republic of Serbia

CONTACT

Tel: +381 36 383 269
+381 36 383 377
+381 36 383 378

Fax: +381 36 383 269

Email: editor@engineering-today.com

Web: www.engineering-today.com

FREQUENCY

4 issues per year

PRINTED BY

Grafika Galeb d.o.o, Niš

CIRCULATION

50 copies/issue

INSTRUCTION FOR AUTHORS

A Engineering TODAY manuscript should by written clearly and concisely in correct English. The length of a reviewing paper is up to 12 pages. All papers are subject to a reviewing process. Final acceptance of a paper for publication in the Journal is based on the decision of the Editorial Board.

TEMPLATE FOR MANUSCRIPT

Template can be downloaded from the journal's website.

SUBMISSION OF PAPERS

All manuscripts for consideration by the Engineering TODAY should be submitted via the journal's website.

CIP - Каталогизација у публикацији
Народна библиотека Србије, Београд

621(497.11)

ENGINEERING Today / editor in chief Radovan Bulatović. - Vol. 1, No. 3 (2022) - . - Kraljevo : The Faculty of Mechanical and Civil Engineering, University of Kragujevac, 2022 - (Niš : Grafika Galeb). - 30 cm

Tromesečno. - Je nastavak: IMK-14 = ISSN 0354-6829. -
Drugo izdanje na drugom medijumu:
Engineering Today (Kraljevo. Online) = ISSN 2812-9938
ISSN 2812-9474 = Engineering Today (Kraljevo)
COBISS.SR-ID 64530953

PROOFREADERS

TECHNICAL EDITORS

AIMS AND SCOPE

Engineering Today is an international peer-reviewed scientific journal that publishes original papers, both theoretical and experimental, covering the whole spectrum of engineering sciences, but focusing mostly on mechanical, electrical and civil engineering. The primary objective is to provide a high-level platform for researchers and practitioners to disseminate theoretical or engineering-oriented research output achievements within the context of engineering systems that fosters knowledge sharing in different branches of engineering discipline.

Engineering Today also publishes novel theoretical methods, algorithms, simulations, experiments, and case studies as applications of state-of-the-art research in the field of engineering.

The topics of interest include, but are not limited to:

- Mechanical engineering
- Electrical/electronic engineering
- Civil engineering
- Manufacturing engineering
- Software engineering
- Thermal technique and environment protection
- Applied mathematics and physics
- Theoretical and applied mechanics
- Optimization algorithms
- Metaheuristic algorithms
- Railway engineering
- Earth-moving, construction and transportation machinery
- Automatic control and fluid technique
- Computer science
- Information systems
- Fault detection and diagnosis
- Learning systems
- Robust systems
- Neuro-fuzzy systems
- Internet of things
- Cybernetics
- System identification
- Stochastic systems
- Complex networks
- Computational complexity
- Mechatronics
- Production technologies
- Computer design and computer integrated processes design
- Design of machining processes
- Engineering management and entrepreneurship
- Mechanical construction and material technology
- Interdisciplinary applications

It provides an effective medium for researchers and a way to quickly publish high-quality original papers, so as to convey the latest important progress in their professional field to scientists in related disciplines. Engineering Today offers authors rigorous peer review, rapid publication, and maximum visibility. The journal expects to accept only the most relevant manuscripts and will provide very rapid evaluation to prevent publication delays. The Editors reserve the right to reject papers without sending them out for review.

From time to time, Engineering Today will publish review articles, short communications, discussions as well as special issues on a specific sub-field of engineering science. Authors are encouraged to contact the Editor-in-Chief if they would like to submit a review article or propose and edit a special issue of the journal.

Engineering
TODAY

VOL. 1 / NO. 3 / 2022

CONTENTS

ORIGINAL SCIENTIFIC PAPER OPEN ACCESS

The application of metaheuristic algorithms in multi-objective optimization of engineering problems

Goran Miodragović[1], Marina Bošković[2*], Radovan Bulatović[2]

[1] Technical College of Applied Studies in Mechanical Engineering, Trstenik, Serbia

[2] University of Kragujevac, Faculty of Mechanical and Civil Engineering in Kraljevo, Kraljevo, Serbia

ARTICLE INFO

[*] **Correspondence:** boskovic.m@mfkv.kg.ac.rs

DOI: 10.5937/engtoday2203007M

UDC: 621(497.11) **ISSN:** 2812-9474

Article history: Received 03 September 2022; Accepted 29 September 2022

ABSTRACT

Comparative testing of three modified metaheuristic algorithms - the cyclic algorithm of the bat family (Loop BFA), the hybrid cuckoo search and the firefly algorithm (H-CS-FA) and the modified krill herd algorithm (MKH)was performed in the paper. The authors tested these algorithms in relation to original ones and the effectiveness of the modifications was confirmed for each individual algorithm. Here, the effectiveness of all three algorithms was verified on two engineering problems in the field of metal cutting - optimization of the body of the turning knife and optimization of the eccentric of the clamping tool. In both cases, multi-objective optimization with two objective functions was performed. By comparing the obtained optimization results as well as the speed of convergence, appropriate conclusions about the efficiency of the algorithms and recommendations for their application were made.

KEYWORDS

Metaheuristic, Multiobjective optimization, Modified algorithms, Turning knife, Eccentric of clamping tool

1. INTRODUCTION

Metaheuristic algorithms are widely used in modern engineering problems. They can be classified into biologically inspired and non-biologically inspired. Bio-inspired algorithms imitate phenomena and processes in nature (e.g. the evolution process), but they also find inspiration in animal systems (flocks of birds, colony of ants, bees, ...). Metaheuristic algorithms are being developed permanently and their number is constantly increasing. A detailed review of existing algorithms was given by Yang [1].

In order to obtain better characteristics of the algorithm, some modifications (improvements) and hybridization of algorithms are carried out. The paper compares the efficiency of three modified biologically inspired algorithms: the cyclic algorithm of the bat family (Loop BFA), the hybrid cuckoo search and the firefly algorithm (H-CS-FA) and the modified krill herd algorithm (MKH). The cyclic algorithm of the bat family (Loop BFA) represents a modification of the standard BA by including the loop search in the zone of solutions [2,19]. H-CS-FA represents a combination of two algorithms and it was used in the optimization of the dynamic quantities of the mechanism which is described in detail in[3, 4]. Modified krill herd algorithm (MKH) proposed by Bulatović et al [5] corresponds to an improved version of the standard krill herd algorithm.

In the text below, the mentioned algorithms will be used in the optimization of machining parameters. The problem of choosing optimal parameters, in order to improve the quality of machining process, reduce costs and increase the

efficiency of production, dates back to the beginning of the XX century. The problem of choosing optimal machining parameters is actually a problem of multi-objective optimization, where the objective functions are often opposed to each other. Namely, it is clear that an increase in quality of machining process requires an increase in machining costs, while an increase in efficiency (use of more robust machining parameters: higher cutting speed, larger step and increased cutting depth) can lead to a decrease in quality of the process of machining. Different methods are used in optimization of machining parameters, from conventional optimization methods (geometric programming, dynamic programming, integer programming) to meta-heuristic algorithms [6-14].

Johari et al. [6] used a hybrid algorithm which combines firefly algorithm and particle swarm optimization to optimize the machining parameters in turning operation. A. R. Yildiz [7] presents a new hybrid optimization algorithm based on the algorithm of differential evolution (DE) and receptors for editing the properties of the immune system, which is applied in the optimization of the milling process. In order to obtain optimal machining parameters pattern search algorithm was applied in [8]. In addition to single-criteria optimization, the authors also use this algorithm for multi-objective optimization when determining the optimal machining parameters for EDM. A methodology based on multi-objective particle swarm optimization algorithm, for identifying the optimal parameters for machining a workpiece with a milling is presented in [9]. To solve the problem of multi-objective optimization when determining the optimal turning parameters, Deb and Datta [11] use the evolutionary multi-objective optimization (EMO) algorithm. In order to obtain better convergence properties, EMO is modified using a procedure of local search. Optimization of multi-pass face milling parameters using six metaheuristic algorithms are described in [13]. Hossain [14] applied five metaheuristic algorithms (Artificial Bee Colony, quick artificial bee colony, modified differential evolution, ant colony optimization and simulated annealing) for solving optimization problem of minimizing the machining time for end milling operation on hot die steel (H13).

The rest of the paper is organized as follows: Section 2 describes the problem of optimization of the body of the turning knife, while the optimization of the eccentric of the clamping tool is described in detail in Section 3. Conclusions are given in Section 4.

2. OPTIMIZATION OF THE BODY OF THE TURNING KNIFE

When machining metal by turning, the separation of the material is caused by the penetration of the cutting wedge of the turning knife into the material of the object of machining. It belongs to the group of oblique cutting, in which the main movement, which is rotary, is performed by the workpiece, while the auxiliary movement is straight and it is performed by the tool[19].

Three main cutting resistances occur during the turning process (Figure 1): F_1- main resistance to cutting, F_2- resistance to the penetration of the cutting wedge of the tool into the workpiece material, F_3 - resistance to auxiliary movement [15]:

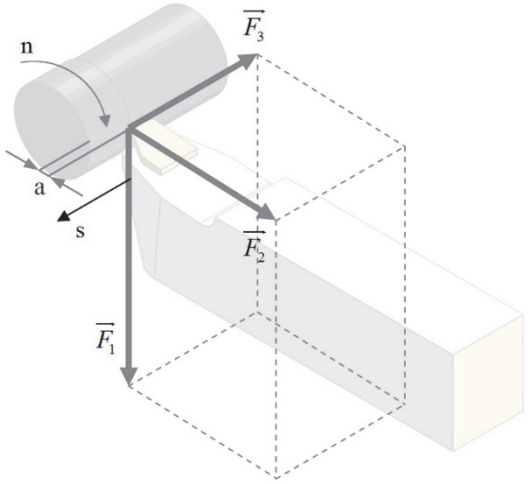

Figure 1: Model of cutting forces in metal turning

The basic parameters of machining process when perform turning are [15]: cutting depth *a*[mm], number of turns of the workpiece *n*[o/min], tool step*s*[mm/o].

The main cutting resistances (Figure 2) can be expressed as a function of the machining parameters, which is represented by equations (1) to (3).

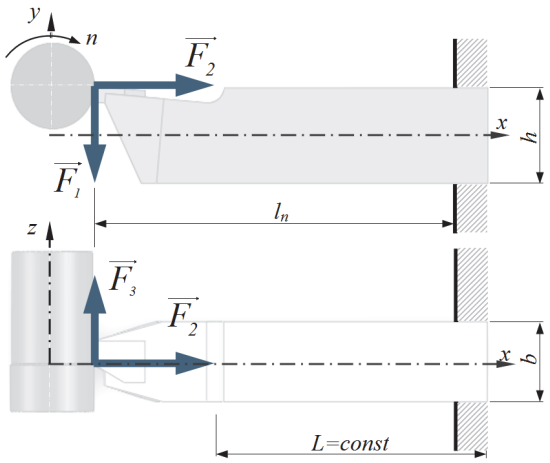

Figure 2: The main cutting resistances in the horizontal and vertical planes

$$F_1 = C_{k1} a^{x_1} s^{y_1} \tag{1}$$

$$F_2 = C_{k2} a^{x_2} s^{y_2} \tag{2}$$

$$F_3 = C_{k3} a^{x_3} s^{y_3} \tag{3}$$

where C_{ki}, x_i and y_i $(i = 1,2,3)$ are factors that depend on the type of workpiece material [15, 16].

Since the turning knife is clamped in the tool holder, it is necessary to check the resistance of the body of the knife to bending and pressure which occurs under the influence of the main resistance to cutting. The expressions for the stresses, which occur in the body of the turning knife, are given by equations (4) - (6).

$$\sigma_x = -\frac{F_2}{A} = -\frac{F_2}{b \cdot h} \tag{4}$$

$$\sigma_y = \frac{M_y}{W_y} \tag{5}$$

$$\sigma_z = \frac{M_z}{W_z} \tag{6}$$

where: σ_x [N/mm^2] is the pressure experienced by the knife body from penetration resistance F_2 [N], σ_y [N/mm^2] is a normal stress due to bending moments about the y-axis M_y [Nmm] - equation (7), W_y [mm^3] is a resisting moment of the knife body section for the y-axis -equation (8), σ_z [N/mm^2] is a normal stress due to bending moments about the z-axis M_z [Nmm] -equation (9), W_z [mm^3] is a resisting moment of the knife body section for the z-axis -equation(10), b, h [mm] are dimensions of the cross-section of the body of the knife.

$$M_y = -F_3 \cdot l_n \tag{7}$$

$$W_y = \frac{b^2 \cdot h}{6} \tag{8}$$

$$M_z = -F_1 \cdot l_n + F_2 \cdot \frac{h}{2} \tag{9}$$

$$W_z = \frac{b \cdot h^2}{6} \tag{10}$$

When equations (7) and (8) are included in equation (5), i.e. when equations (9) and (10) are inserted into equation (6), expressions for σ_y and σ_z represented by equations (11) and (12) will be obtained, respectively.

$$\sigma_y = -\frac{6 \cdot C_{k3} a^{x_3} s^{y_3} \cdot l_n}{b^2 \cdot h} \tag{11}$$

$$\sigma_z = -\frac{6 \cdot C_{k1} a^{x_1} s^{y_1} \cdot l_n}{b \cdot h^2} + \frac{6 \cdot C_{k2} a^{x_2} s^{y_2} \cdot h}{2 \cdot b \cdot h^2} \tag{12}$$

The total normal stress represents the sum of the absolute values of the stress σ_x, σ_y and σ_z, and it must satisfy the criterion of the allowed stress, equation (13).

$$\sigma = |\sigma_x| + |\sigma_y| + |\sigma_z| \leq \sigma_{allowed} \tag{13}$$

Due to the setting of restrictions related to the stress state of the body of the knife in the turning process, this analysis of the load of the body of the turning knife was necessary.

2.1. Objective functions and constraints

The optimization problem refers to the determination of the maximum amount of material during turning processing $MRR = f(v,s,a)$, at the minimum dimensions of the cross-section of the body of the turning knife $V = f(b,h,l_n)$. The mathematical model of the objective function with constraints is given by equations (14)-(20).

$$\max(MRR = v \cdot s \cdot a) \left[\text{mm}^3 / \text{min}\right] \tag{14}$$

$$\min(\text{V} = \text{b} \cdot \text{h} \cdot \text{l}_n) \tag{15}$$

Constraints:

$$g_1 = \sigma - \sigma_{allowed} \leq 0; \tag{16}$$

$$g_2 = F_1 - 2300 \leq 0; \tag{17}$$

$$g_3 = P - P_{\max} \cdot \eta \leq 0; \tag{18}$$

$$g_4 = 1.6 - \frac{h}{b} \leq 0; \tag{19}$$

$$g_5 = 1.6 - \frac{l_n}{h} \leq 0; \tag{20}$$

Multi-objective optimization is defined by equations (14) and (15). Namely, the idea is to choose the machining parameters (cutting speed -*v*, step -*s*, depth of cut –*a*) which will result in the maximum amount of processed material (MRR), while the dimensions of the cross-section of the knife are minimal. In equation (15), the total length of the knife body *L* is not taken into account, because it can be expressed as a function of the free length of the knife l_n and the length necessary for clamping $L = l_n + const$.

The constraint g_2 refers to the recommendation of the maximum cutting force $F_{1\max} = 5000 \left[\text{N}\right]$, while constraint g_3 refers to the maximum cutting power $P_{\max} = 10 \left[\text{kW}\right]$. The data for $F_{1\max}$ and $P_{\max}$, taken from [11], refer to the machining of a steel bar with a turning knife with a P20 plate on a CNC lathe with a motor power of 10kW and a degree of utility $\eta = 75\%$. Constraints g_4 and g_5 refer to the recommended values of the ratio of the dimensions of the cross-section of the knife body, i.e. the ratio of the free length of the knife body l_n and the height of the cross-section *h* [15, 16].

Design variables: cutting speed -*v*, step –*s*, cutting depth -*a*, body dimensions of the turning knife section –*b* x *h* are within the limits:

$$250 \leq v \leq 400;\ 0.15 \leq s \leq 0.55;\ 0.5 \leq a \leq 6 \quad [11]$$

$$6 \leq b \leq 40;\ 6 \leq h \leq 50;\ 9 \leq l_n \leq 80 \quad [16]$$

2.2. Optimization results

A comparative view of the results obtained by the cyclic algorithm of the bat family (Loop BFA), the hybrid cuckoo search and the firefly algorithm (H-CS-FA) and the modified krill herd algorithm (MKH) is given in Table1.

Table1:The optimization results of the body of the turning knife

	LoopFBA		H-CS-FA		MKH	
v	400.00		269.33896		396.54641	
s	0.55		0.15		0.4909	
a	0.8378628547		1.45836		1.55493	
$b\times h\times l_n$	$6\times 11\times 32$		$6\times 49\times 80$		$6\times 10\times 16$	
g_1	-4437.506512054349		-2500.859192700796524		-3796.969160138297	
g_2	-1.250043413696		- 0.578612316356966		-0.370862022226	
g_3	-25.219197149399		-190.310830811429		-22.737268160532	
g_4	-1.309090909091		-0.0326530612244897		0	
g_5	-0.23333333		-6.56666666666667		-0.0666666	
	MRR	V	MRR	V	MRR	V
The best	184329.82803274	2112.00	168511.0910474	2288.00	302692.3929835	960.00
Mean value	183979.56124019	3009.084	165766.029386	3479.672	299723.9669634	2322.4833
The worst	174427.75962776	13230.00	162150.580446	4800.00	242608.23611	13182.434
S.D.	1432.809543	1874.2335	3091.82371	1229.655	5751.79684722	1000.729

It can be seen (Table 1) that the values of the objective functions obtained by the modified krill herd algorithm (MKH) are the best compared to the other two algorithms. Also, the constraint functions $g_i\left(\ i=1,..,6\right)$ are satisfied for all three algorithms, because $g_i \le 0, \forall\ i=1,..,6$.

On the other hand, the fastest convergence is obtained by applying the cyclic algorithm of the bat (LoopFBA), i.e., the best solutions are reached the fastest. With the MKH algorithm, we also have a very fast convergence, and then frequent repetition of values close to or equal to the mean values of the objective functions, so the best results are obtained only at the end of the iterative process

3. OPTIMIZATION OF THE ECCENTRIC OF THE CLAMPING TOOL

Clamping with an eccentric is based on the principle of a wedge - an oblique plane. The eccentric is cylindrical (Figure 3.a) or the plate element (Figure 3.b) revolving around an axis that is placed eccentrically in relation to its axis of symmetry[17].

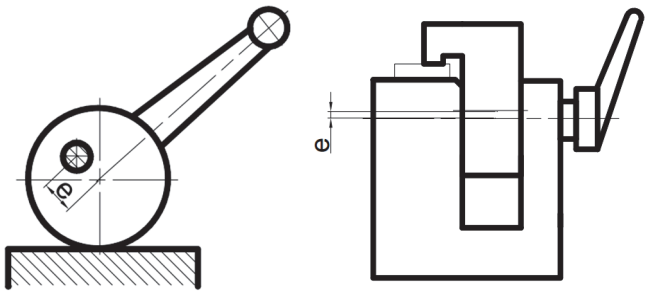

a) b)

Figure3: Examples of eccentrics

Eccentrics are made of case-hardening steel and they are cemented to a hardness of 55-60HRC, while the contact surfaces of the eccentrics are ground. Due to a shorter service path (downward movement of the handle) eccentric clamping is performed in a short time interval. However, eccentrics have a narrower application. They are used in machining operations characterized by high stability of the clamping tool, lower cutting forces and machining with slight vibrations. In principle, there are two types of eccentrics - circular and curvilinear. A circular eccentric was chosen for the optimization problem, while the basic formulas for calculating the eccentric are given below.

One of the basic conditions that the eccentric must satisfy is the provision of self-braking. For this reason, it is necessary to consider the relationships that should be fulfilled in order for the friction angle to be greater than the angle of climb of the eccentric [17].

Looking at Figure 4, it is possible to establish the dependence between the angle of climb of the eccentric - α and the angle of rotation of the eccentric - β, equation (21).

$$\tan\alpha = \frac{e \cdot \cos\beta}{R + e \cdot \sin\beta} \tag{21}$$

where: e – eccentricity, $R = \frac{D}{2}$ - radius of the eccentric.

The clamping force F_s, which is achieved when clamping with a circular eccentric, can be calculated with sufficient accuracy assuming that the eccentric functions as a wedge. In principle, the problem can be presented as a static balance of forces in relation to the point of rotation of the eccentric arm (Figure4).

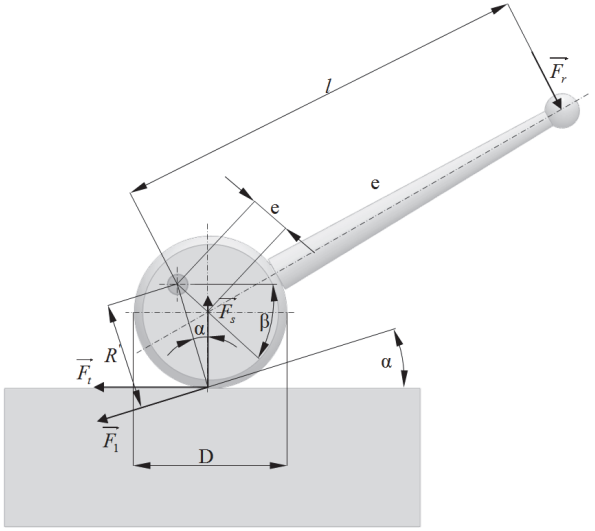

Figure4:Analysis of forces on a circular eccentric

Starting from the equilibrium equation of moments at the point of rotation of the eccentric sleeve (22), i.e., the equation of the distribution of forces at the wedge (23), it will be obtained the dependence of the clamping force on the force on the lever arm of the eccentric (24).

$$F_r \cdot l = F_1 \cdot R', \; F_t = F_1 \cdot \cos\alpha \tag{22}$$

$$F_s = \frac{F_t}{\mathrm{tg}(\alpha + \rho_1) + \mathrm{tg}\rho_2} \tag{23}$$

$$F_s = \frac{F_r \cdot l}{\left[\mathrm{tg}(\alpha + \rho_1) + \mathrm{tg}\rho_2\right] \cdot R'} \tag{24}$$

where: F_r - force on the eccentric lever (it can be adopted~ 150N), l - arm of force [mm], α - variable climbing angle of eccentric [rad], ρ_1 - friction angle on the contact surface of the eccentric and the workpiece [rad], ρ_2 - friction angle on the sleeve of the eccentric [rad], R' - distance of the pivot point of the eccentric from the point of contact $R' = \frac{\frac{D}{2} + e \cdot \sin\beta}{\cos\alpha}$, F_1 - resulting force acting on the object of processing.

3.1. Objective functions and constraints

Based on the previous analysis, an optimization model of the circular eccentric can be set up. In this case, it is a multi-objective optimization with two objective functions. The first objective function refers to determining the minimum dimensions of the eccentric, while the second objective function enables the achievement of the maximum clamping force.

The mathematical model and the corresponding constraint functions are given by equations (25) to (32).

$$\text{Minimize } V = \left(\frac{D}{2}\right)^2 \cdot \pi \cdot b \tag{25}$$

$$\text{Maximize } F_s = \frac{F_r \cdot l}{\left[\operatorname{tg}(\alpha+\rho_1)+\operatorname{tg}\rho_2\right]\cdot R'} \tag{26}$$

Constraints:

$$g_1 = F_R - F_s \le 0 \tag{27}$$

$$g_2 = p_{contact} - \left(p_{contact}\right)_{allowed} \le 0 \tag{28}$$

$$g_3 = \left(p - p_{allowed}\right)_{sleeve} \le 0 \tag{29}$$

$$g_4 = 14 - \frac{D}{e} \le 0 \tag{30}$$

$$g_5 = \frac{18.65 \cdot F_s}{K \cdot D \cdot b} + 41.4 - HRC \le 0 \tag{31}$$

$$g_6 = \left(p - p_{allowed}\right)_{eccentric} \le 0 \tag{32}$$

The constraint g_1 ensures that the clamping force is not less than the maximum cutting force. In this example, it was assumed that the maximum cutting force is $F_R = 2500\text{N}$.

The constraint g_2 checks whether permanent deformations will occur at the point of contact [17]. The contact surface pressure, $p_{contact}$, is calculated according to the equation (32),while the value $\left(p_{contact}\right)_{allowed}$ represents the 20% increased value of the stress at the yield point of the weaker material $\left(p_{contact}\right)_{allowed} = 1.2 \cdot R_e$.

$$p_{contact} = \frac{4}{\pi}\sqrt{\frac{E_e \cdot F_s}{R' \cdot b}} \tag{33}$$

where: $E_e = \frac{2 \cdot E_1 \cdot E_2}{E_1 + E_2}$ - the equivalent Young's modulus of elasticity, E_1, E_2 - Young's modulus of elasticity of eccentric and workpiece, respectively and *b* - width of the eccentric.

Furthermore, it is necessary to check the pressure values obtained on the contact line between the eccentric and the workpiece (equation (34)),as well as the pressure in the sleeve of the eccentric (equation (35)) in relation to allowed pressure values for the materials of the eccentric and the working material $p_{allowed}$ .Since it is steel, the allowed pressure value in this case is $p_{allowed} = 150\left[N/mm^2\right]$.

$$p_{eccentric} = \frac{F_s}{D \cdot b} \tag{34}$$

$$p_{sleeve} = \frac{F_s}{D_r \cdot b} \tag{35}$$

where D_r is the diameter of the sleeve of the eccentric.

Equation (31) refers to the checking of surface deformation according to Levin and Reshetov, for line contact. In this equation, *K*represents the permissible contact load, which depends on the type of thermal treatment (fully hardened or cemented then hardened; induction hardened or nitrided) and on the type of contact (ball, short roller, long roller).For induction-hardened surfaces and a short roll $K = 18\left[N/mm^2\right]$, while $HRC = 96.4$ for steel Č3130.

Design variables: diameter of the eccentric - *D*, eccentric - *e*, angle of rotation of the eccentric - β, force arm - l, width of the eccentric - b and diameter of the sleeve of the eccentric - D_r are within the limits [18]:

$$40 \le D \le 115;\quad 4 \le e \le 10;\quad 30 \le \beta \le 90;\quad 60 \le b \le 120;\quad 15 \le D_r \le 35$$

3.2. Optimization results

A comparative view of the results obtained by the cyclic algorithm of the bat family (Loop BFA), the hybrid algorithm of the cuckoo search and firefly algorithm (H-CS-FA) and the modified krill-herd algorithm (MKH) is given in the Table2.

Table2: The results of the optimization of the eccentric

	LoopFBA		H-CS-FA		MKH	
D	56.00007347098426		68.86583		56.22869	
E	4		4.00000		4.01169	
B	90° (π/2)		90°(π/2)		85°(π·17/30)	
l	164.3		180.00000		174.13285	
B	10.039361		96.00000		110.47683	
D_r	31.0841824131		35.00000		20.12035	
g_1	-562.3928		-293.665770918547		-598.8392358535625	
g_2	-0.1095		-38.5151961538239		-1.3786958795177	
g_3	-149.0965		-149.168551853893		-148.6059051886784	
g_4	-0.0012		-3.2164575		-0.0162101259070	
g_5	-54.4804		-54.56216975549		-54.4831360914344	
g_6	-149.4985		-149.577429254628		-149.5011501150574	
	V	F_s	V	F_s	V	F_s
The best	268610.06705	3062.39278	292348.91465	2975.81491	274332.3369382	3098.8395451
Mean value	268930.13266	3058.82352	323218.03655	2815.65655	277164.7488624	3039.7645054
The worst	275779.70696	2996.54577	423905.92624	2231.86118	295327.5310168	2933.7663861
S.D.	707.52216565	6.56736132	45435.2027358	266.058509	2191.683067381	42.749816778

It can be seen, from the table above, that the highest clamping force is obtained by the MKH algorithm, while the smallest volume is obtained by applying the LoopFBA algorithm. All constraints $g_i \ (i=1,..,6)$ are satisfied because $g_i \le 0, \forall\ i=1,..,6$.

4. CONCLUSION

The application of three biologically inspired algorithms- the cyclic algorithm of bat (LoopFBA), the hybrid algorithm of the cuckoo search and firefly algorithm (H-CS-FA) and the modified krill-herd algorithm (MKH)was tested in this paper. Testing of modified algorithms was performed on the examples of optimization of the body of the turning knife and eccentric.

Based on the obtained results, it can be concluded that the mentioned algorithms function correctly. Convergence is good, with a high value of standard deviation for both examples and all three algorithms. This can be explained by the fact that it is a multi-objective optimization of two contradictory objective functions. In the first example, the minimum dimensions of the body of the turning knife were requested, but with the achievement of the maximum amount of removed material during the machining. In the second example, the objective function was to achieve the maximum clamping force while obtaining the minimum dimensions of the eccentric.

Comparing the results, for both examples, it can be concluded that the MKH algorithm gives better results than the other two algorithms.

In the example of the optimization of the turning knife body, the MKH algorithm gave significantly better results than the Loop BFA and H-CS-FA algorithm (Table1). Unlike Loop BFA, MKH algorithm converged relatively quickly, but towards a value close to or equal to the mean value of the objective function, only to achieve the best result at the end of the iterative process.

A similar conclusion can be drawn for the example of optimization of the eccentric. The highest clamping force was obtained by using the MKH algorithm, while Loop BFA gives the smallest dimensions of eccentric with the achievement of a satisfactory clamping force (Table 2). The results obtained by the H-CS-FA algorithm are worse than the other two mentioned algorithms. Unlike the Loop BFA, the MKH algorithm converged relatively quickly to a value close to the mean value of the objective function, only to achieve the best result in the last third of the iterative process.

REFERENCES

[1] X.S. Yang and H. Xingshi, "Nature-inspired optimization algorithms in engineering: Introduction and Overview", Nature Inspired Computation in Engineering, pp. 1-20, https://doi.org/10.13140/RG.2.2.24609.56167, (2016)

[2] G. Miodragović and R. Bulatović, "Loop bat family algorithm (Loop BFA) for constrained optimization", Journal of Mechanical Science and Technology, Vol.29, pp. 3329-3341, https://doi.org/10.1007/s12206-015-0730-9, (2015)

[3] M. Bošković, R. Bulatović, S. Šalinić, G. Miodragović and G. Bogdanović, "Optimization of dynamic quantities of a four-bar mechanism using the Hybrid Cuckoo Search and Firefly Algorithm (H-CS-FA)", Archive of Applied Mechanics, Vol.88, pp. 2317-2338, https://doi.org/10.1007/s00419-018-1457-8, (2018)

[4] M. Bošković, "Modern approachesin kinematic and dynamic optimization of planar mechanisms", PHD thesis, University of Kragujevac (Serbia), (2019)

[5] R. Bulatović, G. Miodragović and M. Bošković, "Modified Krill Herd (MKH) algorithm and its application in dimensional synthesis of a four-bar linkage", Mechanism and Machine Theory, Vol.95, pp. 1-21, https://doi.org/10.1016/j.mechmachtheory.2015.08.004, (2016)

[6] N. F. Johari, A. M. Zain, N. H. Mustaffa and A. Udin, "Machining Parameters Optimization using Hybrid Firefly Algorithm and Particle Swarm Optimization", The 6th International Conference on Computer Science and Computational Mathematics (ICCSCM 2017), Journal of Physics: Conference Series, Langkawi (Malaysia), Vol. 892, 4–5 May (2017)

[7] A.R. Yildiz, "A new hybrid differential evolution algorithm for the selection of optimal machining parameters in milling operations", Applied Soft Computing, Vol. 13, pp. 1561– 1566, https://doi.org/10.1016/j.asoc.2011.12.016, (2013)

[8] M. Madić and M. Radovanović, "Optimization of machining processes using pattern search algorithm", International Journal of Industrial Engineering Computations, Vol. 5, pp. 223– 234, https://doi.org/10.5267/j.ijiec.2014.1.002, (2014)

[9] O.O. Villegas, C.F. Espinoza et al., "A Methodology for Optimizing the Process of Machining a Workpiece Using Multi-Objective Particle Swarm Optimization", Research in Computing Science, Vol. 132, pp. 33-40, https://doi.org/10.13053/rcs-132-1-3, (2017)

[10] R.V. Rao and V.D. Kalyankar, "Parameter optimization of modern machining processes using teaching-learning-based optimization algorithm", Engineering Applications of Artificial Intelligence, Vol. 26, pp. 524–531, https://doi.org/10.1007/s00170-012-4524-2, (2013)

[11] K. Deb and R. Datta, "Hybrid Evolutionary Multi-Objective Optimization of Machining Parameters", Engineering Optimization, Vol. 44, pp. 685-706, https://doi.org/10.1080/0305215X.2011.604316, (2012)

[12] N. Yusup, A. Sarkheyli, A.M. Zain, S.Z.M. Hashim and N. Ithnin, "Estimation of optimal machining control parameters using artificial bee colony", Journal of Intelligent Manufacturing, Vol. 25, pp. 1463-1472, https://doi.org/10.1007/s10845-013-0753-y, (2014)

[13] S. Diyaley and S. Chakraborty, "Optimization of multi-pass face milling parameters using metaheuristic algorithms", FACTA UNIVERSITATIS Series: Mechanical Engineering, Vol. 17, No 3, pp. 365 – 383, https://doi.org/10.22190/FUME190605043D, (2019)

[14] Md S. J. Hossain and T.W. Liao, "Cutting Parameter Optimization for End Milling Operation Using Advanced Metaheuristic Algorithms", International Journal of Advanced Robotics and Automation, Vol.2, pp. 1-12, https://doi.org/10.15226/2473-3032/2/2/00125, (2017)

[15] M. Kalajdžić, "Tehnologija obrade rezanjem – priručnik", University of Belgrade, Faculty of Mechanical Engineering, Belgrade (Serbia), (2004)

[16] D. Milikić i drugi, "Tehnologija obrade rezanjem, zbirka rešenih i zadataka za vežbu", University of Novi Sad, Faculty of Technical Sciences, Novi Sad (Serbia), (2000)

[17] B. Tadić, "Alati i pribori, skripta", University of Kragujevac, Faculty of Mechanical Engineering, Kragujevac (Serbia), (2008)

[18] D. Pajić, "Konstrukcija i primena steznih alata", Tehnička knjiga, Beograd (Serbia), (1967)

[19] G. Miodragović, "Advanced bio-inspired algorithms development for solving optimization problems in applied mechanics", PHD thesis, University of Kragujevac (Serbia), (2016)

ORIGINAL SCIENTIFIC PAPER OPEN ACCESS

The elimination of the anti-coincidence colorimetry in the process of painting the shell of a vehicle by applying WCM

Jelena Jovanović[1], Branimir Živanović[2], Aleksandar Jovičić[3*], Nedeljko Dučić[3], Ivan Milićević[4], Marko Popović[4]

[1] University of Kragujevac, Faculty of Technical Sciences /Department of Industrial Management, Čačak, Serbia

[2] Vorverk Autotec Serbia, Čačak, Serbia

[3] University of Kragujevac, Faculty of Technical Sciences/Department of Mechatronics, Čačak, Serbia

[4] University of Kragujevac, Faculty of Technical Sciences/Department of Mechanical Engineering, Čačak, Serbia

ARTICLE INFO

[*] **Correspondence:** aleksandar.jovicic@ftn.kg.ac.rs

DOI: 10.5937/engtoday2203017J

UDC: 621(497.11) **ISSN:** 2812-9474

Article history: Received 14 September 2022; Accepted 29 September 2022

ABSTRACT

This work presents the optimization of process of car shell painting in FCA Serbia Ltd. by using the world class manufacturing (WCM). In order to show the advanced Kaizen within the pillar "Focused improvement" we have taken an example of problems in the production of a passenger vehicle "Fiat 500L" which is reflected in an inadequate colour match during serial production. The anticoincidence in the process of painting the shell of a vehicle was eliminated by Kaizen method. The analysis of vehicle shell painting process improvement was carried out by DOE, the verification of the proposed activities was completed, the experiment factor was identified, a hypothesis testing was conducted, all results were viewed and the process of verification and optimization was completed.

KEYWORDS

World Class Manufacturing, The elimination of anticoincidence, The process of painting

1. INTRODUCTION

Most worldwide manufacturing industries due to the increasing market competency and economic crisis are seeking solutions to improve their performances. The two most significant strategies (models) which are used by companies are Lean Production and World Class Manufacturing. The similarities and differences between these two manufacturing strategies are described in details in this work [1]. At a very detailed level, the lean production practices include but not limited to practices such as cellular manufacturing, multifunctional workforce, lot size reduction, just-in-time (JIT), work delegation, total productive maintenance (TPM), set up time reduction, total quality management (TQM), continuous flow production, agile manufacturing strategies, safety improvement programs, process capability measurement and human resource management [2]. Of course, not all companies are ready to apply contemporary models, so in support to this, the authors in this work propose a model on assessing the maturity of the organizations when applying WCM system [3]. Various consultants have started implementing their own versions of Toyota's production system under Western names such as Continuous Flow Manufacturing, Inventory-free manufacturing, and World Class Manufacturing [4].

Model WCM (World class Manufacturing) world class production based on 10 interconnected technical pillars related to the production process and which, due to the easier understanding and monitoring, are presented and defined through seven steps. Beside technical, WCM consist of 10 managerial colums which are evaluated during the review as a subjective perception of the examiner. WCM was developed in the 1920s by Hausan, Schonberger and other authors. They determined that the measuring methods of the quality of manufacturing organizations at the time, especially those which carry out production by working orders, (MTO-Make to order) no longer gave good results and it was necessary to develop a new concept that, in addition to the more realistic description of the process, enables benchmarking on a global scale[5,6]. The management of the organization according to WCM principles is based on high-quality reliable methods and tools in the wide involment of all employees and company management. The mere adoption of such an approach allows accomplishing high-quality and measurable savings in the production process [7]. In Serbia, this concept is most often used in foreign companies, with international or combined management, where changes in the competitiveness of any organization are monitored on a monthly basis. This work will show the optimization of the process of painting the shell of vehicles in FCA Serbia Ltd. by applying WCM governance model. Precisely, process optimization using WCM management model is the goal of the work, practical implementation and problem solving using the Kaizen approach and methodology is a possible contribution of the work.

2. BASICS OF THE WCM

The WCM principles are applied to all aspects of the organization, from quality systems to maintenance, from cost control to logistics to constant improvement. WCM system is based on the systematic reduction of all types of costs and losses through the benefits of all employees and with the precise use of the methods, standards and tools that world class production requires.

Each of the technical pillars must achieve a specific goal, which is supported by the managerial pillars. Managerial pillars are prescribed the requirements which are necessary in order to obtain better working conditions and improvement of technical pillars. Each technical pillar, following the prescribed standards must go through seven steps, where in each it is necessary to fulfill certain tasks in order for the pillar to move to the next level. Although this is about different pillars with different goals, they are closely related to each other and one without the other cannot manage. So, for example, the Safety pillar aims to eliminate accidents, the Cost Deployment pillar aims to identify problems related to the costs and points out where the major problems are, so that everyone can focus on eliminating them, the Focused Improvement pillar develops new insights and reduces the costs by using appropriate methods, the Workplace organization and Autonomous maintenance aims to increase the level of the competency of the people in the facility by organizing the workplace where the greatest costs are and where intensive work is needed, and by autonomous maintenance in parts with large investments in equipment. Thus, pillars are like the links of the chain, attach to each other and with their corporation provide support to the WCM temple. The ten management pillars form the foundation of the WCM:

Dedication – If the plans of the boards of directors are unaware or do not support management in order to achieve a level of world-class performance, company is doomed. 2) Involvement- All people in the company must be aware of the goals and tasks of the business. They must also be a key factor that will enable companies achieve their goals through their actions. 3) Communication- Before people can commit to this concept, they need to be informed about it in detail. People need to understand how and why WCM is important to the decisions of the company's goals. 4) Understanding – Understanding what and where the problems are is the starting point for making improvements. 5) Measurement - Measurement is the key in qualifying problems and determing their priorities, as well as determing the efficiency of the improvements achieved. It is necessary to perform a performance measurement before and after the changes and in that way determine weather and to what extent the changes of performances have improved. 6) Scheduling - Scheduling refers to how goals are converted to actions. 7) Application - Implementation of the right solutions to identified problems by applying strict principles with the help of trained people is essential for success. People can also learn and improve when implementing solutions. 8) Assessment - The assessment needs to be an integral part of the improvement process to see if the problem and solution have been solved. 9) Standardization – When the evaluation cycle is over, it is the time to standardize the method of process management, so that the obtained result is maintained after solving the problem, not that we have the same problem again. 10) Documentation – Documentation is created in order to accumulate the degree of knowledge and to use them in other areas in the future.

The quality pillar is responsible for carrying out quality studies. In the world class manufacturing model, the "Quality Control" (QC) pillar focuses on determining process conditions, maintaining predetermined conditions and ensuring production compliance to prevent nonconformities (Szewieczek, Roszak and Helizanowicz, 2008).

In WCM system, it is necessary to first identify the problems that will be considered, than determine the location and prioritize them by the cost analyses. After that, it is necessary to determine the right methods and evaluate how much the solution costs. It is necessary to implement solutions with accuracy and evaluate the achieved results in relation

to the original goal. To solve the problem WCM tools are used that can be divided into three groups: tools for describing the problems, tools for finding the root of the sample and tools for the standardization of the results.

When a problem arises, it is necessary to describe it with the use of appropriate tools. Using the tool 5W+1H we describe the problem by filling out a standardized form. After the description, it is moved to search for a sample problem with the help of a tool 4M (Men, Machine, Material, Method) that uses a herringbone diagram to show all possible causes of the problem, whereby the same is shared with those produced by man, machine, method and material. After generating all possible samples using no check list, the circle of possible causative agents is narrowed.

Finally, for the remaining possible samples, the depth of the problem is entered bu using the tool 5W – question "Why?", at least five time, we determine the actual cause of the problem [8].

3. FOCUS IMPROVEMENT

The purpose of the third technical pillar is to eliminate the main loss previously identified within the steps for the distribution and analysis of costs. In this way, organizations do not use resources for problematic issues of lower priority. Corrective actions are targeted and must lead to the final resolution of the problem and the renewal or introduction of a new specific standard. Focused on improvements make seven steps:

Step 1: Defying a model of a zone or machine within which continuous improvement will be carried out. Zones can be parts of production that are recognized as bottlenecks or zones that produce large losses.

Step 2: Stratification loss is carried out, and, that is, a breakdown is carried out into all types of losses.

Step 3: Choosing a project to be done and defying the activities of the project itself. When we talk about the tool that will be implemented in order to solve a particular problem, we use "Kaizen".

An example of good practice of using the Lean-Kaizen concept is described by the authors in their work [9].

3.1. KAIZEN

Kaizen is a method of continuous improvement. A substantive translation would mean a change for the better that everyone is doing every day at all levels in one company. Kaizen comes from the best practice of Japanese management, it is dedicated to improving productivity, efficiency, quality and business excellence at all. Small improvements that apply to key processes, generate an increase in profits while gaining client loyalty. The purpose of this method is to exceed the stated goals of one company.

Step 4: Creating a team based on their competencies that will work on the project depending on the complexity of the problem.

Step 5: Defines the work on the implementation project in seven steps: Defining the problem. Classification of potential causes of the problem. Detecting the real or true causes of the problem. Establishing a definite solution to a given problem. Implementation of the solution. Verification of solutions and monitoring of the results. Standardization of a certified solution. Analysis of the cost-effectiveness of the project. Solution verification and horizontal expansion.

Step 6: Cost-benefit analysis of the project's profitability.

Step 7: Verification of the solution and its horizontal expansion [10, 11].

4. ELIMINATION OF ANTICOINCIDENCE IN COLORIMETRY IN THE PROCESS OF CAR SHELLPAINTING BY APPLYING ADVANCE KAIZEN

In order to display Advance Kaizen within the pillar "Focused Improvement", an example of a problem has been taken within the production of a passenger vehicle "Fiat 500L" which is reflected in an inadequate color match during serial production. Due to the data protection in the continuation of the work, the color will be qualified as a "Specific color ". After the improvement of internal standards in the automotive industry, new methods have been defined about checking the harmonization of the color of the finished product. The method previously applied was based on the visual perception of the controller who was tasked with verifying the harmony of colors (compared to a master pattern) with reflection at the corner of 25°,45° and 75°, that is, (Face, Flash, Flop) as shown in the figure 1 [12].

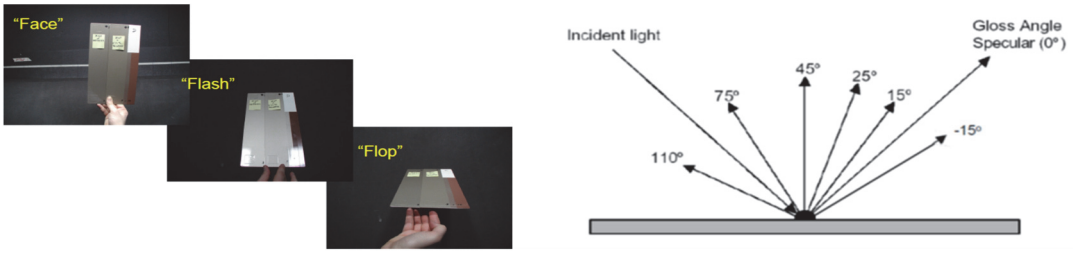

Figure 1: Previous method certification of color harmony on a vehicle.

The new method of checking the color alignment on the finished product is reflected in the measurement of the specific color using device "BTC MAC" which is pressed on the painted surface and by measuring it calculates the difference between the absolute value and the defined standard, figure 2.

a)

b)

Angle	L*	a*	b*	c*
-15°	125.31	-0.92	1.27	1.57
15°	118.87	-0.71	1.24	1.43
25°	100.25	-0.66	0.23	0.70
45°	68.10	-0.65	-0.84	1.07
75°	46.21	-0.73	-1.20	1.40
110°	38.19	-0.91	-1.26	1.56

c)

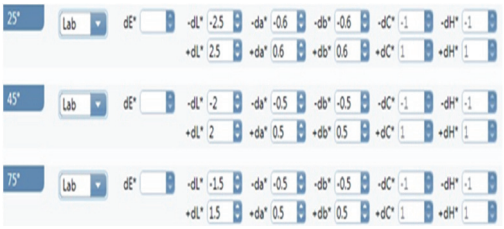

Figure 2: A new method certification of color harmony on a vehicle (a) - measuring device "BYC MAC", b) - measured values, c) – defined standards [12].

What was observed using the device is that the shell of the vehicle is darker than the bumpers of the vehicle, which were painted in an independent process in relation to the shell of the vehicle, figure 3.

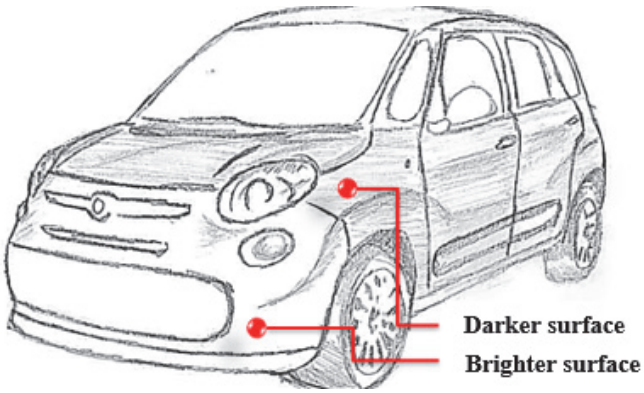

Figure 3: A sketched view of the vehicle effect.

Although the problem was related only to a "specific color", it occupied a high position in the classification of qualitative problems by using "Quality Assurance Matrix", shown in Table 1.

The Quality matrix is the main tool for establishing a quality control in WCM methodology. The purpose of the tool is to find correlation between the non-compliance of products from the process itself, as well to priorities the problems, that is, critical processes based on the criticality index.

The criticality index is calculated by multiplying four multipliers, which are defined by values from 1 to 5 for each individually:

- The frequency of occurrence, that is, the repetition of the problem.
- The cost of direct and indirect materials as well as working hours spent on troubleshooting.
- Detection problem, that is, the location where the defect was detected (if the defect is reported by the buyer, its severity is greater than the defect defected in the production process).
- Problem severity. If the problem affects the general security of the user or affects the ability to perform basic functions, the problem will carry more weight than if we talk about aesthetic problems [13].

INDEX=FREQUENCY×COSTS×DETECTION×SEVERITY

Table 1: A view of problem classification and position within the "QA" Matrix.

#	Input	Source	Component	Anomaly	Frequency	Mat. Cost.	Cost.	Seventy	Detection	Priority Index	Responsibility
32	CPA	Internal	Paint Body Color	Color matchining	2	2	2	4	4	40	PAINT

4.1. Analysis and corrective actions to improve the dyeing process of vehicle shells.

The defect is generated during the painting process "specific color" in the painting booth and it is detected at the final check in the paint shop during spectrophotometer measuring. The painting of outer surface of the vehicle is performed using a robot in the spray booth, through paint bells that are located in the processes of the basic color 1 and 2. (Base Coat 1 and Base Coat 2), so that there is no men's effect to generate problems. After measuring the colorimetry on the vehicle, it was observed that the parameters per L*axis deviate from the specification, that is, the shells of the vehicle tend towards a darker shade as in figure 4 (data is processed in the "Minitab") [13].

Silver_Metallk		dE*			L*			a*			b*			C*			h		
D65/10		25	45	75	25	45	75	25	45	75	25	45	75	25	45	75	25	45	75
Absolute Values					100.25	68.1	46.21	-0.66	-0.65	-0.73	0.23	-0.84	-1.2	0.7	1.07	1.4	160.48	232.2	238.63
Limit / Tol					2.5	2	1.5	0.6	0.5	0.5	0.6	0.5	0.5						
Limit / Tol					-2.5	-2	-1.5	-0.6	-0.5	-0.5	-0.6	-0.5	-0.5						
CheckZone	Status	dE*			dL*			da*			db*			dC*			dH*		
		25	45	75	25	45	75	25	45	75	25	45	75	25	45	75	25	45	75
Match to Std																			
Hauba_Centar	Fail	1.25	0.48	0.75	-2.63	-2.21	-1.72	-0.12	-0.19	-0.14	0.21	0.24	0.11	0.2	-0.03	-0.01	-0.14	-0.3	-0.17
Hauba_Desno	Fail	1.98	1.64	2.73	-2.78	-2.14	-1.68	0.04	-0.08	-0.06	-0.15	0.10	0.01	-0.07	-0.03	0.02	0.13	-0.13	-0.06
Hauba_Levo	Fail	0.28	1.29	1.03	-2.59	-2.15	-1.75	0.02	-0.06	-0.03	-0.12	0.05	0.03	-0.05	0	0	0.11	-0.08	-0.04
Krov_Desno_Nazad	Fail	2.22	1.39	1.63	-2.67	-2.18	-1.63	-0.15	-0.18	-0.14	0.42	0.37	0.14	0.33	-0.11	-0.03	-0.28	-0.39	-0.19
Krov_Levo_Napred	Fail	1.62	0.58	0.61	-2.80	-2.09	-1.66	-0.19	-0.27	-0.17	0.43	0.35	0.11	0.37	-0.02	0.01	-0.27	-0.43	-0.2
Poklopac_Rezervoara	Fail	2.75	2.02	1.99	-2.66	-2.13	-1.62	0.01	-0.08	-0.03	0.03	0.10	-0.05	0	-0.02	0.06	-0.03	-0.13	0
Pr_Desna_Vrata	Fail	0.68	1.22	0.87	-2.71	-2.12	-1.59	-0.09	-0.16	-0.10	0.26	0.27	0.12	0.2	-0.06	-0.05	-0.18	-0.3	-0.15
Pr_Desni_Blatobran	Fail	3.52	1.6	3.16	-3.58	-2.33	-1.82	-0.09	-0.15	-0.13	0.14	0.28	0.12	0.14	-0.08	-0.02	-0.1	-0.3	-0.17
Pr_Leva_Vrata	Fail	0.42	0.77	0.2	-2.81	-2.15	-1.67	-0.15	-0.18	-0.11	0.34	0.29	0.15	0.29	-0.06	-0.06	-0.22	-0.33	-0.17
Pr_Levi_Blatobran	Fail	3.12	1.7	2.82	-3.69	-2.38	-1.86	-0.04	-0.12	-0.08	0.07	0.21	0.04	0.06	-0.07	0.01	-0.05	-0.23	-0.09
V_Vrata_Desno	Fail	0.84	0.5	0.4	-2.61	-2.13	-1.71	0.01	-0.10	-0.08	-0.08	0.12	0.07	-0.03	-0.02	-0.01	0.08	-0.15	-0.11
V_Vrata_Levo	Fail	1.85	0.84	0.12	-2.58	-2.10	-1.73	0.18	0.02	0.02	-0.13	0.06	0.05	-0.21	-0.06	-0.05	0.07	-0.02	-0.01
Za_Desna_Vrata	Fail	0.84	1.37	1.22	-2.71	-2.18	-1.65	-0.15	-0.20	-0.12	0.29	0.30	0.16	0.25	-0.05	-0.06	-0.18	-0.35	-0.19
Za_Desni_Blatobran	Fail	0.31	1.21	0.55	-2.66	-2.17	-1.68	-0.06	-0.13	-0.05	0.17	0.17	0.05	0.13	-0.03	-0.02	-0.13	-0.21	-0.07
Za_Leva_Vrata	Fail	0.8	0.87	0.18	-2.74	-2.18	-1.71	-0.10	-0.16	-0.08	0.30	0.24	0.13	0.23	-0.06	-0.06	-0.21	-0.28	-0.14
Za_Levi_Blatobran	Fail	0.23	0.74	0.08	-2.65	-2.21	-1.66	-0.04	-0.11	-0.03	0.15	0.15	0.06	0.1	-0.04	-0.03	-0.12	-0.18	-0.06

Figure 4: The results of measurements of a non-compliant product.

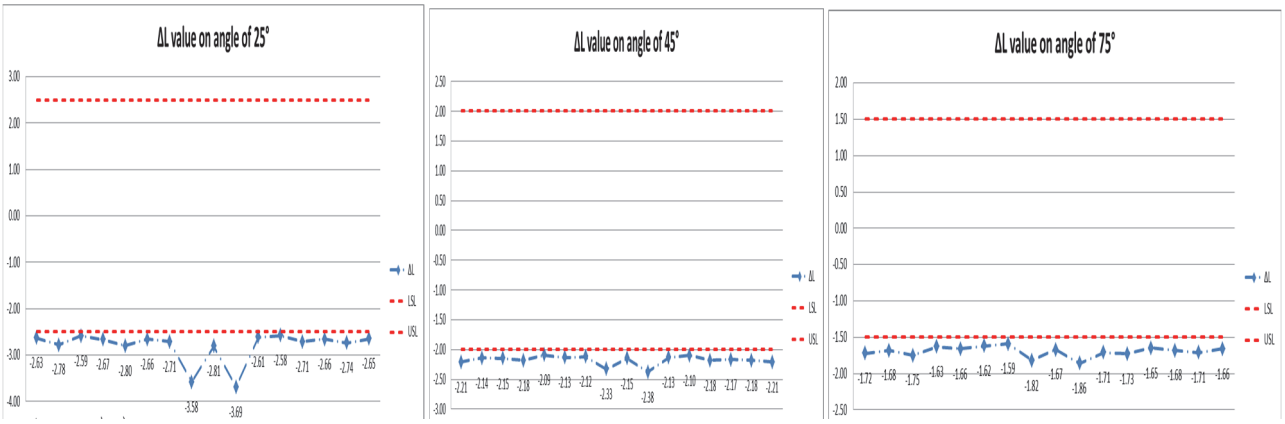

Figure 5: Distribution of measured values for the "specific color" L* characteristics for the angle of 25°, 45° and 75°.

Optional values indicate that the application of paint applications uniformed throughout the product, but that it is outside the set control limit (LSL - lover specific limit, USL - upper specific limit), (figure 5). Also, based on the collected data, it was found that the defect is chronic and is present only on the "specific color" of the vehicle, which accounts for 8,5 % of the total production (figure 6).

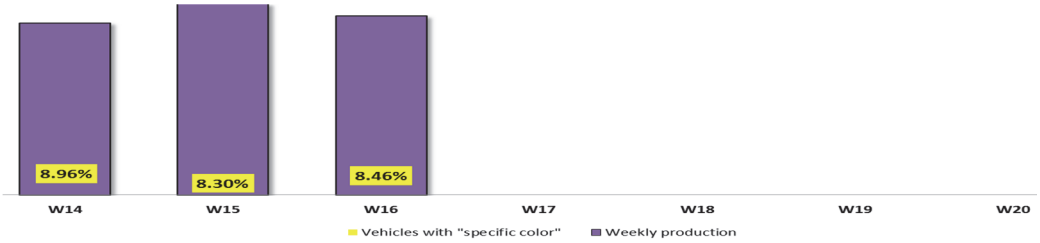

Figure 6: Percentage of product non-compliance in relation to production volume for 3 weeks is shown.

In the continuation of the analysis, the verification of all the basic elements related to the process of painting was carried out, taking into account the 4M analysis, that is, the causative agent of the problems associated with man, machine, method and material, what is shown in the chart.

Table 2: Verification of the basic elements of the process using 4M analysis.

4M	Activities	Status
MAN	Operator is following parameters of robots?	OK
	Operator is respecting AM cycle?	OK
	Operator checking parameters of spray booth?	OK
	Operator is checking parameters of BC and CC according to procedure?	OK
MACHINE	Robot bell?	OK
	Nozzles?	OK
	Shaping air ring?	OK
	Atomizer?	OK
	Dozing pump?	OK
	Pressure regulator?	OK
	Pump for mixing in preparation tank?	OK
	High tension controller?	OK
MATERIAL	Viscosity of material?	OK
	Expire data of material?	OK
	Temperature of material?	OK
	Spectrophotometry of material?	KO
METHOD	Paint preparation?	OK
	Tempering?	OK
	Application parameters?	OK
	Parameters of BC and CC booths?	OK
	Oven parameters?	OK
	Flash off BC1-BC2?	OK
	Method of measurement check?	OK

The discrepancy found during 4M verification was referred to direct material. When delivering paints for serial production, the supplier of materials performs the delivery of colored panels that are painted by simulating the industrial environment with the delivered color. Using "BYC MAC" four panels were measured for the last four deliveries for the specific parameters *L, a ,b* where it was found that in the direct material there was a deviation from the specific parameters *L** and for the angles of 25°, 45° and 75° as shown in figure 7 (data is processed in the "Minitab").

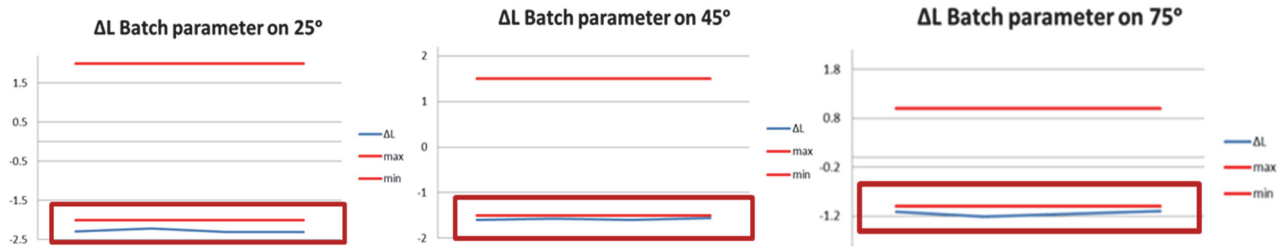

Figure 7: Results of color testing for the last four deliveries by suppliers.

4.2. Verification of actions and defying new activities.

After the report of non-compliance, preventive measures were carried out, i.e. color correction in the production system by adding additives, a re-measurement of the finished product was carried out (figure 8). As a definite solution, a modification of the formula for the preparation of paint in the production process of the supplier.

2h

Silver_Metalik		dE*			L*			a*			b*			C*			h		
D65/10		25	45	75	25	45	75	25	45	75	25	45	75	25	45	75	25	45	75
Absolute Values					100.25	68.1	46.21	-0.66	-0.65	-0.73	0.23	-0.84	-1.2	0.7	1.07	1.4	160.48	232.2	238.63
Limit / Tol					2.5	2	1.5	0.6	0.5	0.5	0.6	0.5	0.5						
Limit / Tol					-2.5	-2	-1.5	-0.6	-0.5	-0.5	-0.6	-0.5	-0.5						
CheckZone	Status	dE*			dL*			da*			db*			dC*			dH*		
		25	45	75	25	45	75	25	45	75	25	45	75	25	45	75	25	45	75
SAMPLE 001	Pass	1.64	0.69	0.73	-1.55	-0.67	-0.32	0.06	-0.11	-0.03	0.54	-0.14	-0.05	0.28	0.18	0.6	-0.46	0	0.26

12h

Silver_Metalik		dE*			L*			a*			b*			C*			h		
D65/10		25	45	75	25	45	75	25	45	75	25	45	75	25	45	75	25	45	75
Absolute Values					100.25	68.1	46.21	-0.66	-0.65	-0.73	0.23	-0.84	-1.2	0.7	1.07	1.4	160.48	232.2	238.63
Limit / Tol					2.5	2	1.5	0.6	0.5	0.5	0.6	0.5	0.5						
Limit / Tol					-2.5	-2	-1.5	-0.6	-0.5	-0.5	-0.6	-0.5	-0.5						
CheckZone	Status	dE*			dL*			da*			db*			dC*			dH*		
		25	45	75	25	45	75	25	45	75	25	45	75	25	45	75	25	45	75
Match to Std																			
SAMPLE 001	Pass	0.42	0.11	0.21	0.13	0.12	-0.11	0.01	-0.07	0	0.03	0.09	0.02	0	-0.02	-0.01	-0.04	-0.11	-0.01

24h

VR 612 Silver_Metalik		dE*			L*			a*			b*			C*			h		
D65/10		25	45	75	25	45	75	25	45	75	25	45	75	25	45	75	25	45	75
Absolute Values					100.25	68.1	46.21	-0.66	-0.65	-0.73	0.23	-0.84	-1.2	0.7	1.07	1.4	160.48	232.2	238.63
Limit / Tol					2.5	2	1.5	0.6	0.5	0.5	0.6	0.5	0.5						
Limit / Tol					-2.5	-2	-1.5	-0.6	-0.5	-0.5	-0.6	-0.5	-0.5						
CheckZone	Status	dE*			dL*			da*			db*			dC*			dH*		
		25	45	75	25	45	75	25	45	75	25	45	75	25	45	75	25	45	75
Match to Std																			
SAMPLE 001	Pass	0.13	0.61	0.23	0.42	0.6	0.23	0.03	-0.06	0.01	-0.03	0.07	-0.03	-0.04	-0.01	0.02	0.02	-0.09	0.02

Figure 8: Test setting, parameters of the measured value for the L parameter.

After verifying the sample and confirming that the paint used in the process is within the specification, the entire shell of the vehicle was re-measured and it was found that there is still a deviation for the parameter L* but in this case it was present only in the positions of the front fender of the vehicle and only for the angle of 25 degrees, as shown in the figure 9.

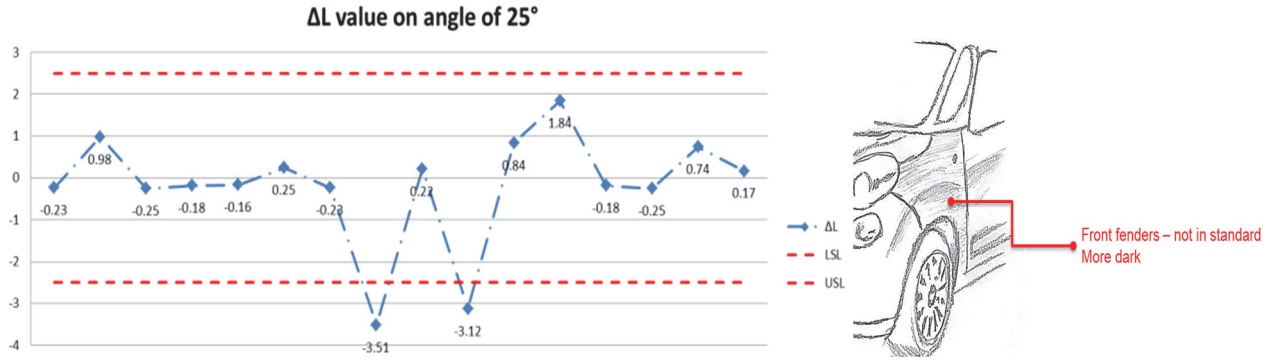

Figure 9: The results of measurement of the entire product after color modification.

Taking into account that all elements of the process were within the specifications, the result of the product was unsatisfactory, it was approached to optimizing the process in order to achieve results and eliminate discrepancies by continuing DOE (Design Of Experiment) project.

4.3. Identification of the experiment factor

As already noted in this work, the entire process of painting the exterior of the vehicle is performed using a robot in the paint cabin (Spray Booth), taking into account that the current non-compliance is related to the front mudguards of the vehicle. This surface of the vehicle shell is painted by robots "R11- Base Coat 1(BC1), and robot "R13"- Base Coat 2 (BC")"- as shown in figure 10.

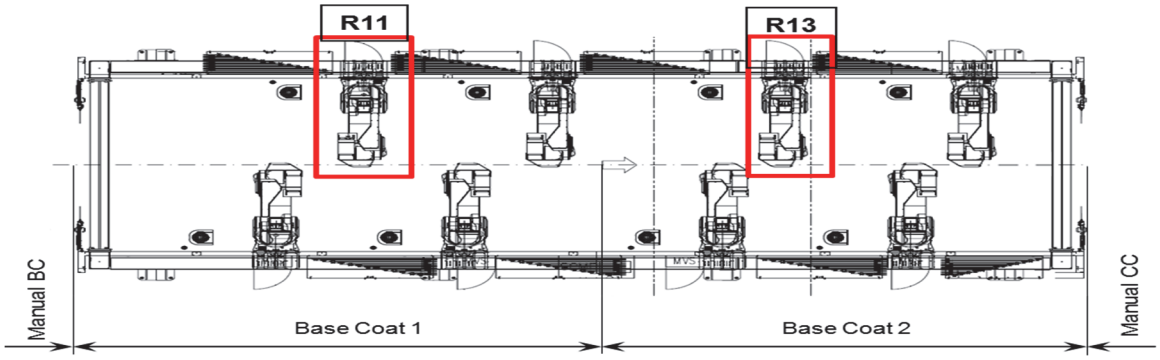

Figure 10: The position of the robot R11 and R13 within the automatic painting process.

In addition to the specific input parameters of the process, there are parameters that are controlled and are under constant monitoring: the viscosity of color and paint temperature, there are also factors that are not controlled and

that have no impact, defined as process noises, air humidity inside the booth and temperature of the spray booth which together form one process system that affects the formation of colorimetry of products.

4.3.1 Hypothesis test

In the continuation of the work, minimum and maximum input parameter values for all factors are defined (Table 3). Since there are 8 factors in total on two levels with two repetitions in case a full testing plan is applied, DOE will be 2^8=256, with two repetitions which is 512 testings in total.

Table 3: display of the minimal and maximum operating parameters (two levels) of input factors.

FACTORS	ACRONYM	MIN Value	MAX Value
Paint Value BC1	PV-BC1	165 ml	180 ml
Shaping Air BC1	SA-BC1	80	120
Turbine Speed BC1	TS-BC1	40000 rpm	60000 rpm
High Voltage BC1	HV-BC1	40 kV	50kV
Paint Value BC2	PV-BC2	110 ml	170 ml
Shaping Air BC2	SA-BC2	380	390
Turbine Speed BC2	TS-BC1	40000 rpm	60000 rpm
High Voltage BC2	HV-BC2	40 kV	50 kV

Taking into account the total number of necessary tests to perform full testing, cost-effectiveness is called into question, time it takes to spend on testing, therefore, it was decided to implement a difficult move in order to eliminate factors that do not have statistical significance.

That is, zero hypothesis and alternatives with a reliability index a= 0.05 (if there is p< 0.05 statistical difference, that is, it represents the probability that hypothesis may be correct) is defined, as shown in Table 4.

Table 4: Defining a zero and alternative hypothesis.

FACTORS	H_0	H_1
PV-BC1	There is no impact PV BC1 on ΔL parameter	There is impact PV BC1 on ΔL parameter
SA-BC1	There is no impact SA BC1 on ΔL parameter	There is impact SA BC1 on ΔL parameter
TS-BC1	There is no impact TS BC1 on ΔL parameter	There is impact TS BC1 on ΔL parameter
HV-BC1	There is no impact HV BC1 on ΔL parameter	There is impact HV BC1 on ΔL parameter
PV-BC2	There is no impact PV BC2 on ΔL parameter	There is impact PV BC2 on ΔL parameter
SA-BC2	There is no impact SA BC2 on ΔL parameter	There is impact SA BC2 on ΔL parameter
TS-BC2	There is no impact TS BC2 on ΔL parameter	There is impact TS BC2 on ΔL parameter
HV-BC2	There is no impact HV BC2 on ΔL parameter	There is impact HV BC2 on ΔL parameter

On the sample of the 14 shells, the measured colorimetry status for parameter L* was subsequently changed for each of the 8 factors and compared with the first measurement using t-test (all data is processed in the "Minitab").

The results of the measurement of the base paint 1 (Basic Coat 1 – BC1) booth for factors "Paint Value", "Shaping Air", "Turbine Speed" and "High Voltage", after measurement showed that all factors have a significant impact on the parameter L* except for the "Turbine Speed", i.e. the obtained values p<0.05, as shown in figure 11.

Paired T-Test and CI: Before, After for Paint Value BC1

```
Paired T for Before - After

            N     Mean   StDev  SE Mean
Before     14  -3.4357  0.0804   0.0215
After      14  -2.4529  0.0578   0.0155
Difference 14  -0.9829  0.0853   0.0228

95% CI for mean difference: (-1.0321, -0.9336)
T-Test of mean difference = 0 (vs ≠ 0): T-Value = -43.09  P-Value = 0.002
```

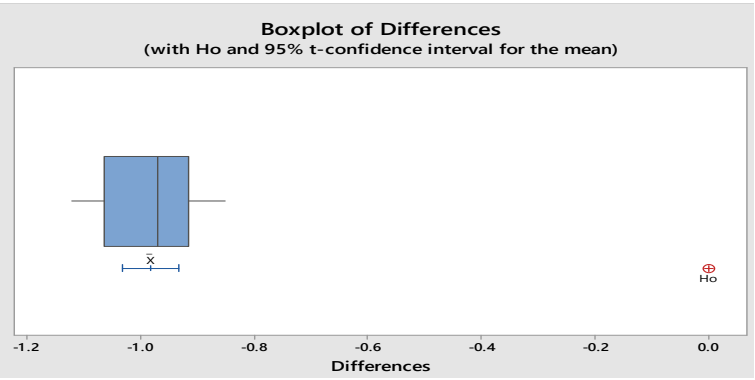

Paired T-Test and CI: Before, After for Shaping

Paired T for Before - After

	N	Mean	StDev	SE Mean
Before	14	-3.4357	0.0804	0.0315
After	14	-2.6245	0.0725	0.0194
Difference	14	-0.8113	0.1019	0.0272

95% CI for mean difference: (-0.8701, -0.7524)
T-Test of mean difference = 0 (vs ≠ 0): T-Value = -29.80 P-Value = 0.012

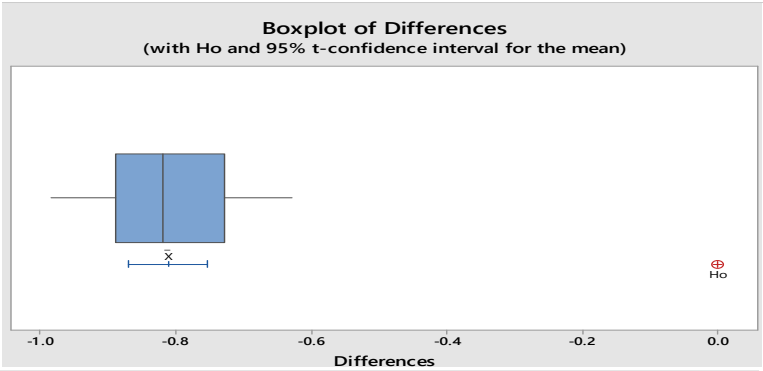

Paired T-Test and CI: Before, After for High Voltage BC1

Paired T for Before - After

	N	Mean	StDev	SE Mean
Before	14	-3.436	0.080	0.021
After	14	-1.364	0.456	0.122
Difference	14	-2.072	0.489	0.131

95% CI for mean difference: (-2.354, -1.790)
T-Test of mean difference = 0 (vs ≠ 0): T-Value = -15.86 P-Value = 0.038

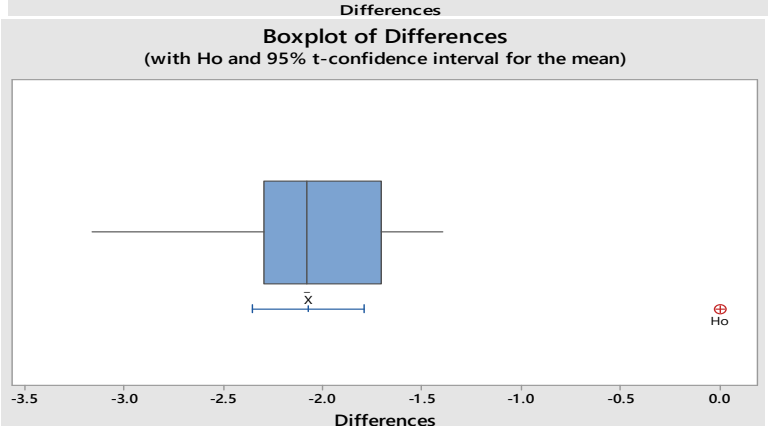

Figure 11: Display of results and t-tests for factors inside the base color 1 booth (Basic Coat 1-BC1).

The results of the measurement of the base paint 2 (Basic Coat 2 – BC2) booth for factors "Paint Value", "Shaping Air", "Turbine Speed" and "High Voltage", after measurement showed that only factor "Paint Value" has a significant influence on the parameter L*, that is the obtained values $p<0.05$, as shown in figure 12.

Paired T-Test and CI: Before, After for Paint Value BC2

Paired T for Before - After

	N	Mean	StDev	SE Mean
Before	14	-3.436	0.080	0.021
After	14	-1.395	0.467	0.125
Difference	14	-2.041	0.499	0.133

95% CI for mean difference: (-2.329, -1.752)
T-Test of mean difference = 0 (vs ≠ 0): T-Value = -17.56 P-Value = 0.021

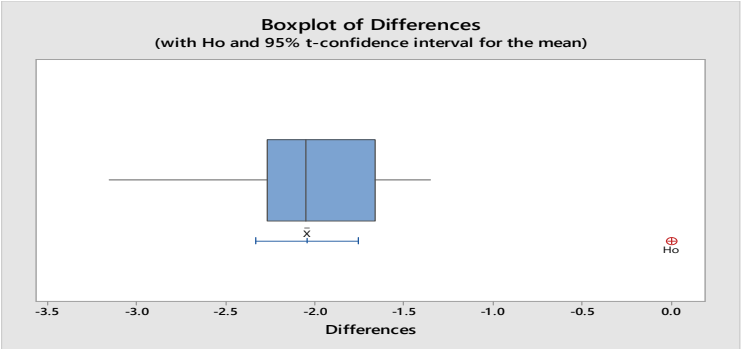

Figure 12: Display of t-test results for factors inside the base paint 2 booth (Basic Coat 2 – BC2).

4.3.2 Fractional Factorial

After the hypothesis test, all relevant input factors that have statistical significance in terms of parameter L* have been identified. These factors will be the basis in the future development of the DOE project and creation of the "Fraction Factorial".

Within the program "Minitab", launching of the DEO has been executed, as shown in figure 13, with an option that the planned tests "½ fraction" i.e. "fraction factorial" by two repetitions would increase the number of tests performed and the sensitivity of the experiment itself in order to identify a correlation between factors [14].

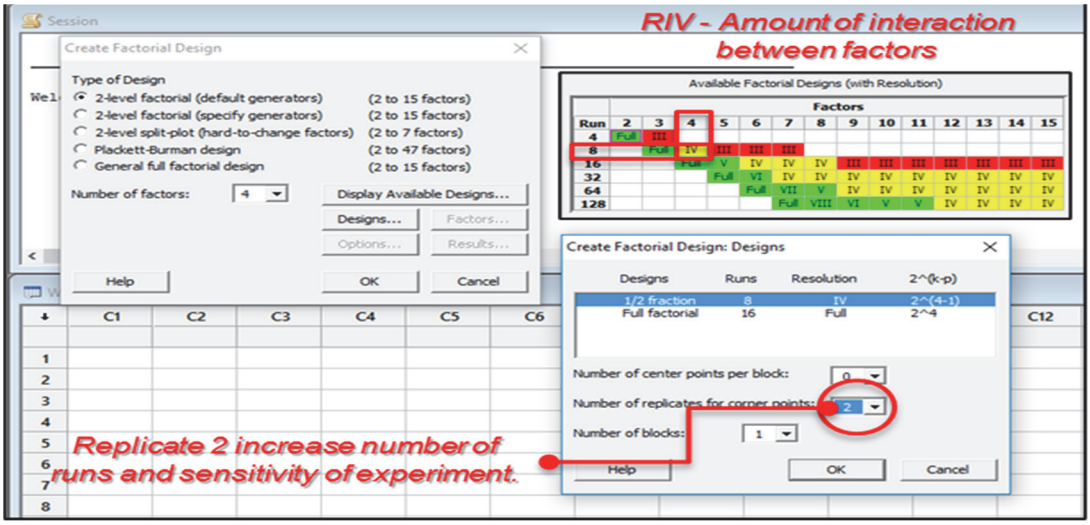

Figure 13: The experiment setting within the program.

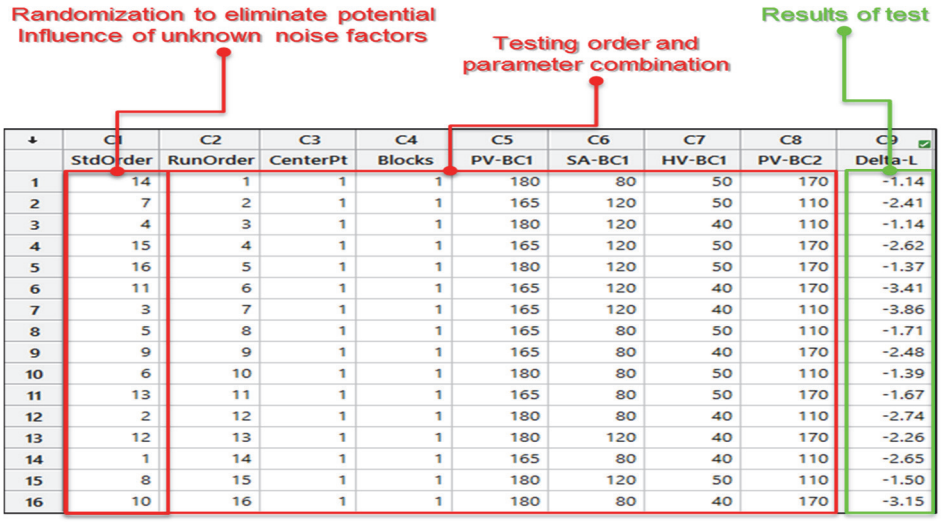

	C1 StdOrder	C2 RunOrder	C3 CenterPt	C4 Blocks	C5 PV-BC1	C6 SA-BC1	C7 HV-BC1	C8 PV-BC2	C9 Delta-L
1	14	1	1	1	180	80	50	170	-1.14
2	7	2	1	1	165	120	50	110	-2.41
3	4	3	1	1	180	120	40	110	-1.14
4	15	4	1	1	165	120	50	170	-2.62
5	16	5	1	1	180	120	50	170	-1.37
6	11	6	1	1	165	120	40	170	-3.41
7	3	7	1	1	165	120	40	110	-3.86
8	5	8	1	1	165	80	50	110	-1.71
9	9	9	1	1	165	80	40	170	-2.48
10	6	10	1	1	180	80	50	110	-1.39
11	13	11	1	1	165	80	50	170	-1.67
12	2	12	1	1	180	80	40	110	-2.74
13	12	13	1	1	180	120	40	170	-2.26
14	1	14	1	1	165	80	40	110	-2.65
15	8	15	1	1	180	120	50	110	-1.50
16	10	16	1	1	180	80	40	170	-3.15

Figure 14: The test setting, parameters and the measured values for the L* parameter.

In the figure 14 are shown the basic elements of the test setting, the test sequence (column C2), factor parameters (column C2:C8) as well as the measured values for each of the tests. (column 9).

4.4. Perceiving the obtained results and optimizing the process

Based on the regression of factors, i.e. analysis, the variations between factors, it was found that the factors of the value of color "paint value", as well as the voltage "high voltage" have the greatest influence on the output parameters of the testing of L* (figure 15) [15].

Factorial Regression: Delta-L versus PV-BC1, SA-BC1, HV-BC1, PV-BC2

Analysis of Variance

Source	DF	Adj SS	Adj MS	F-Value	P-Value
Model	7	8.7864	1.25520	5.80	0.012
Linear	4	6.4205	1.60513	7.42	0.008
PV-BC1	1	2.3409	2.34090	10.82	0.011
SA-BC1	1	0.1681	0.16810	0.78	0.404
HV-BC1	1	3.8809	3.88090	17.95	0.003
PV-BC2	1	0.0306	0.03062	0.14	0.716
2-Way Interactions	3	2.3659	0.78862	3.65	0.064
PV-BC1*SA-BC1	1	2.2052	2.20523	10.20	0.013
PV-BC1*HV-BC1	1	0.0006	0.00063	0.00	0.958
PV-BC1*PV-BC2	1	0.1600	0.16000	0.74	0.415
Error	8	1.7300	0.21625		
Total	15	10.5164			

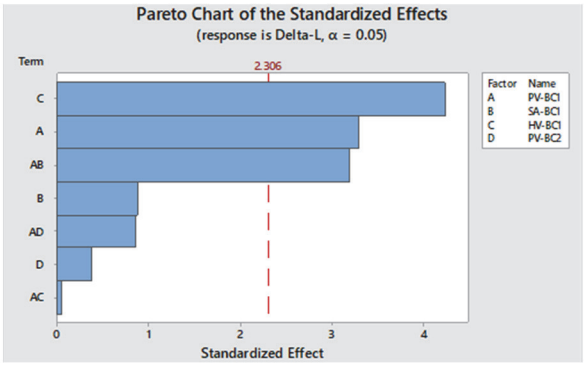

Figure 15: Regression of factors and their influence on the output parameter of testing L*

Based on all collected data within the software program "Minitab", a platform for optimizing parameters was launched in order to achieve the best results, that is, to make the output by optimizing the output value as close as possible to nominal requirements "Hit a target value" and to achieve as much of the desired index "Desirability Index-a" as possible, as shown in figure 16.

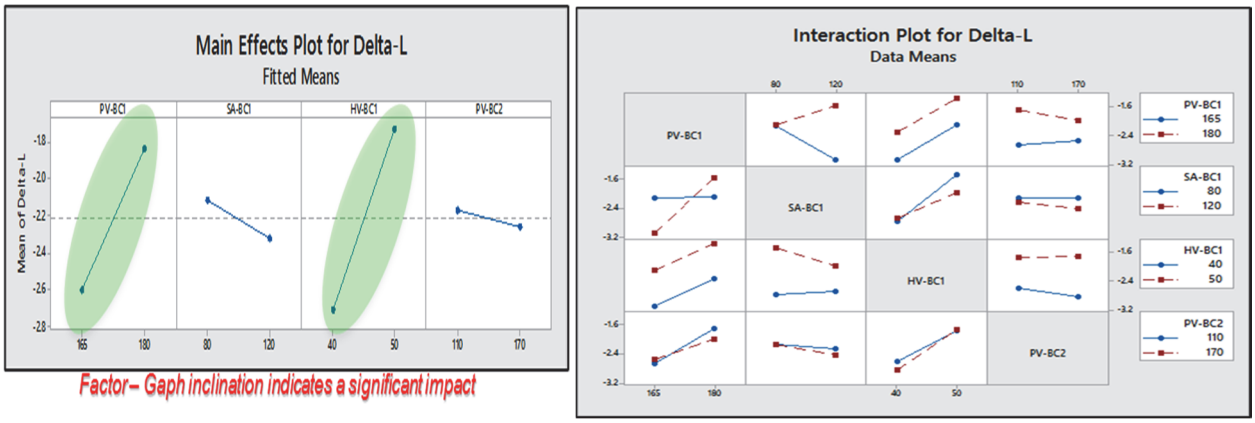

Figure 16: The effect of plot the influence of parameters, their interaction, relative to the output parameter of testing L*.

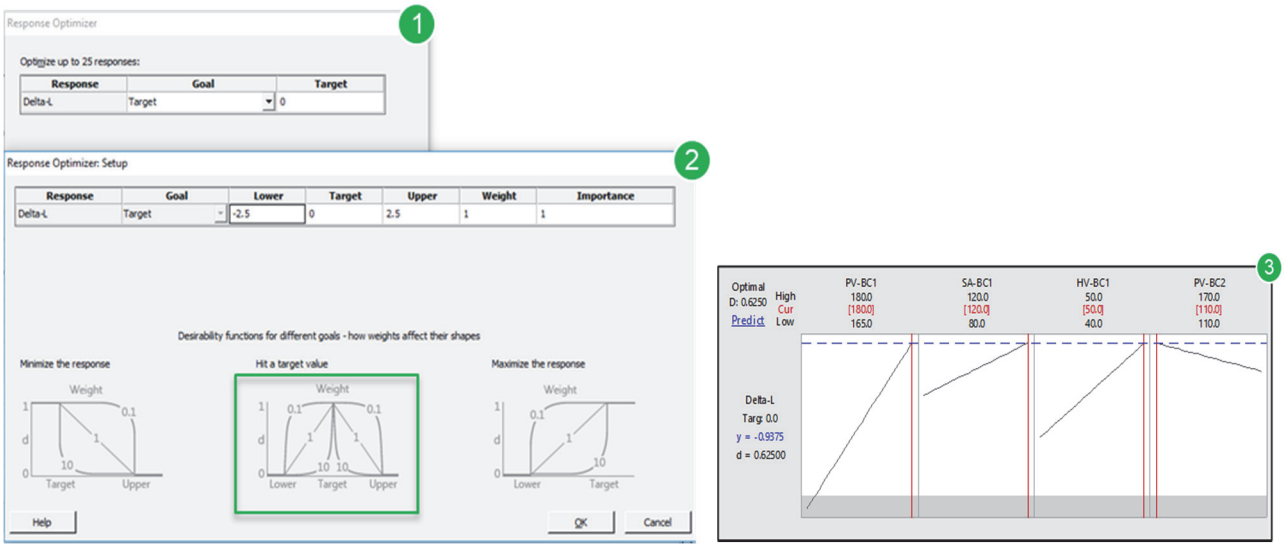

Figure 17: Parameter optimization using the "Minitab" software package

4.5. Product verification based on process optimization

After the software modification, a physical modification of the process parameters was also performed, as shown in the table 5.

Table 5: Setting of process parameters after more applications of this optimization are completed.

FACTORS	ACRONYM	RUN TEST1	RUN TEST 2
Paint Value BC1	PV-BC1	180 ml	
Shaping Air BC1	SA-BC1	120	
Turbine Speed BC1	TS-BC1	40000 rpm	60000 rpm
High Voltage BC1	HV-BC1	50kV	
Paint Value BC2	PV-BC2	110 ml	
Shaping Air BC2	SA-BC2	380	390
Turbine Speed BC2	TS-BC1	40000 rpm	60000 rpm
High Voltage BC2	HV-BC2	40 kV	50 kV

Performing a confirmatory experiments is the rule of completion of DOE, in the case of a partial experiment it is even essential. The validation of the experiment must include and eliminate factors whose main goal is to avoid wrong decisions due to the small number of tests performed. Figure 18 shows the validation results of that test [16].

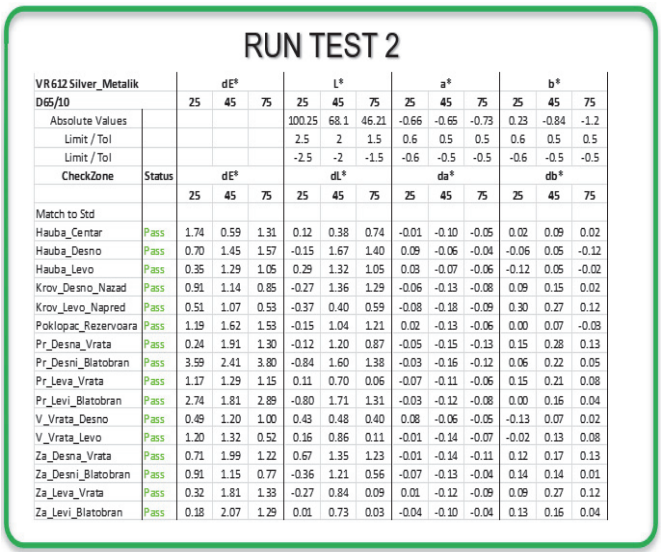

RUN TEST 2

VR612 Silver_Metalik		dE*			L*			a*			b*		
D65/10		25	45	75	25	45	75	25	45	75	25	45	75
Absolute Values					100.25	68.1	46.21	-0.66	-0.65	-0.73	0.23	-0.84	-1.2
Limit / Tol					2.5	2	1.5	0.6	0.5	0.5	0.6	0.5	0.5
Limit / Tol					-2.5	-2	-1.5	-0.6	-0.5	-0.5	-0.6	-0.5	-0.5
CheckZone	Status	dE*			dL*			da*			db*		
		25	45	75	25	45	75	25	45	75	25	45	75
Match to Std													
Hauba_Centar	Pass	1.74	0.59	1.31	0.12	0.38	0.74	-0.01	-0.10	-0.05	0.02	0.09	0.02
Hauba_Desno	Pass	0.70	1.45	1.57	-0.15	1.67	1.40	0.09	-0.06	-0.04	-0.06	0.05	-0.12
Hauba_Levo	Pass	0.35	1.29	1.05	0.29	1.32	1.05	0.03	-0.07	-0.06	-0.12	0.05	-0.02
Krov_Desno_Nazad	Pass	0.91	1.14	0.85	-0.27	1.36	1.29	-0.06	-0.13	-0.08	0.09	0.15	0.02
Krov_Levo_Napred	Pass	0.51	1.07	0.53	-0.37	0.40	0.59	-0.08	-0.18	-0.09	0.30	0.27	0.12
Poklopac_Rezervoara	Pass	1.19	1.62	1.53	-0.15	1.04	1.21	0.02	-0.13	-0.06	0.00	0.07	-0.03
Pr_Desna_Vrata	Pass	0.24	1.91	1.30	-0.12	1.20	0.87	-0.05	-0.15	-0.13	0.15	0.28	0.13
Pr_Desni_Blatobran	Pass	3.59	2.41	3.80	-0.84	1.60	1.38	-0.03	-0.16	-0.12	0.06	0.22	0.05
Pr_Leva_Vrata	Pass	1.17	1.29	1.15	0.11	0.70	0.06	-0.07	-0.11	-0.06	0.15	0.21	0.08
Pr_Levi_Blatobran	Pass	2.74	1.81	2.89	-0.80	1.71	1.31	-0.03	-0.12	-0.08	0.00	0.16	0.04
V_Vrata_Desno	Pass	0.49	1.20	1.00	0.43	0.48	0.40	0.08	-0.06	-0.05	-0.13	0.07	0.02
V_Vrata_Levo	Pass	1.20	1.32	0.52	0.16	0.86	0.11	-0.01	-0.14	-0.07	-0.02	0.13	0.08
Za_Desna_Vrata	Pass	0.71	1.99	1.22	0.67	1.35	1.23	-0.01	-0.14	-0.11	0.12	0.17	0.13
Za_Desni_Blatobran	Pass	0.91	1.15	0.77	-0.36	1.21	0.56	-0.07	-0.13	-0.04	0.14	0.14	0.01
Za_Leva_Vrata	Pass	0.32	1.81	1.33	-0.27	0.84	0.09	0.01	-0.12	-0.09	0.09	0.27	0.12
Za_Levi_Blatobran	Pass	0.18	2.07	1.29	0.01	0.73	0.03	-0.04	-0.10	-0.04	0.13	0.16	0.04

Figure 18: Positive results of validation of new process parameters.

Table 5: new setup of machine was done based on the test and observed results.

FACTORS	BEFORE	AFTER	FACTORS	BEFORE	AFTER
PV-BC1	165 ml	180 ml	PV-BC2	170 ml	110 ml
SA-BC1	80	120	SA-BC2	380	380
TS-BC1	40000 rmp	40000 rmp	TS-BC1	40000 rmp	40000 rmp
HV-BC1	40 kV	50 kV	HV-BC2	50 kV	50 kV

	1st	2st
	ΔL	ΔL
Pr_Desni_Blato-bran	-0,82	-0,84
Pr_Levi_Blatobran	-0,78	-0,8

5. CONCLUSION

World-class production is an operational strategy that, if well applied, gives a new dimension of production that corresponds to the rapid inclusion of new high-quality products. In this paper WCM strategy was applied to optimize the process of painting the shell of vehicles in FCA Serbia ltd.

The practical contribution of the paper is related to problem solving of inadequate color matching during serial production on the example of production of a "Fiat 500L" passenger vehicle was solved. By applying DOE, through the Kaizen method, the non-compliances of colorimetry were eliminated and the process of painting the shell of the vehicle was improved, after which the verification of proposed solutions and optimization of the mentioned process were carried out.

The theoretical contribution is reflected in the definition of the world class manufacturing (WCM) methodology for the elimination of nonconformities in the automotive industry. The limitations of the work are reflected in the small number of repetitions of the experiment, so future directions of research should be in this sense.

ACKNOWLEDGEMENTS

Authors of this work thank to the company FCA Serbia for helping with the realization of this work. This study was supported by the Ministry of Education, Science and Technological Development of the Republic of Serbia.

REFERENCES

[1] F. De Carlo and G. Simioli, "Lean production and world class manufacturing: a comparative study of the two most important production strategies of recent times", International Journal of Industrial and Operations Research, Vol. 1 (1), pp. 1-16, http://dx.doi.org/10.35840/IJIOR/6501, (2018)

[2] S. Sahoo and S. Yadav, "Lean production practices and bundles: a comparative analysis", International Journal of Lean Six Sigma, Vol. 9 (3), pp. 374-398, https://doi.org/10.1108/IJLSS-01-2017-0002, (2018)

[3] C.T.A. de Andrade, A.P.H. de Gusmão and W. Silva, "World class manufacturing performance measurement using a maturity model and the flowsort method", International Journal of Production Research, Vol. 59 (24), pp. 7374-7389, https://doi.org/10.1080/00207543.2021.1970845, (2021)

[4] Y. Goshime, D. Kitaw and K. Jilcha, "Lean manufacturing as a vehicle for improving productivity and customer satisfaction: A literature review on metals and engineering industries", International Journal of Lean Six Sigma Vol. 10 (2), pp. 691-714, https://doi.org/10.1108/IJLSS-06-2017-0063, (2019)

[5] L. Hendry, "Applying world class manufacturing to make-to-order companies: problems and solutions", International Journal of Operations & Production Management, Vol. 18(11), pp. 1086-1100, https://doi.org/10.1108/01443579810231679, (1998)

[6] B. Maskell, "Performance Measurement for World Class Manufacturing", Productivity Press, Portland (USA), (1991)

[7] K. P. Faculty, "World Class Manufacturing model in production management", Archives of Materials Science and Engineering Vol. 58(2), pp. 227-234, (2012)

[8] S. Arsovski and I. Đokić, "Quality and World Class Manufacturing", 38. Nacionalna konferencija o kvalitetu, Mašinski fakultet Univerziteta u Kragujevcu, Kragujevac (Srbija), 19-21 Maj, p.51, (2011)

[9] S. Kumar, A.K. Dhingra, and B. Singh, "Application of lean-kaizen concept for improving quality system of manufacturing firms", International Journal of Industrial Engineering: Theory, Applications, and Practice, Vol 28 (5), https://doi.org/10.23055/ijietap.2021.28.5.3540 , (2022)

[10] FIAT Group – Manufacturing training unit,"WCM Kick Off", Education Conference in Vrnjacka Banja, Vrnjacka Banja (Srbija), 3-4 November, (2009)

[11] FIAT Group, "World Class Manufacturing –Methods and Tools", Torino (Italy), April (2006)

[12] H. Yamashina, "Safety" WCM Academy, Kragujevac (Serbia), (2012)

[13] FCA Serbia, "Training material – QA Matrix", WCM Academy, Kragujevac (Serbia), (2017)

[14] H. Yamashina, S. Ketter and L. Massone, "Audit Evaluation Guide" WCM development center, Turin (Italy), (2016)

[15] FIAT Group – Manufacturing training unit, "WCM Approach Extended 1st Edition", Unite, Turin (Italy), (2010)

[16] H. Yamashina and T. Kubo, "Manufacturing cost deployment", International Journal of Production Research, Vol. 40 (16), pp. 4077- 4091, https://doi.org/10.1080/00207540210157178, (2002)

ORIGINAL SCIENTIFIC PAPER OPEN ACCESS

Pushover analysis for upgrading of existing residential masonry building

Saša Marinković[1*], Bojan Milošević[1, 2], Žarko Petrović[3], Dušan Turina[2], Davorin Penava[4]

[1] University of Kragujevac, Faculty of Mechanical and Civil Engineering, Kraljevo, Serbia

[2] Academy of Technical and Art Applied Studies Belgrade/School of Civil Engineering and Geodesy, Belgrade, Serbia

[3] University of Niš, Faculty of Civil Engineering and Architecture/Department of Civil Engineering, Niš, Serbia

[4] Josip Juraj Strossmayer University of Osijek, Faculty of Civil Engineering and Architecture Osijek, Croatia

ARTICLE INFO

[*] **Correspondence:** marinkovic.s@mfkv.kg.ac.rs

DOI: 10.5937/engtoday2203031M

UDC: 621(497.11) **ISSN:** 2812-9474

Article history: Received 16 September 2022; Accepted 10 October 2022

ABSTRACT

Masonry is common used for classic building construction, but is known for its seismic vulnerability. The existing regulations in Serbia (Eurocode) demand control of the behaviour of masonry buildings exposed to seismic actions. For this it is most convenient to use, for engineering purposes, non-linear static (pushover) analysis. With the aim of increasing knowledge about the seismic behavior of different structural configurations created by upgrading an existing residential two-story masonry building, a comparative study was conducted on four different proposed models. This paper presents the most significant results of pushover analyses performed on a spatial model of the structure of the existing building that needs to be upgraded and on spatial models of the structures with an additional floor level and different positioning of vertical confining elements while evaluating their seismic capacity in compliance with the regulations. Two different lateral load distributions are assumed in computation since the appropriate lateral load profile is not always obvious. Based on various approaches, there are different identified responses.

KEYWORDS

Masonry building, Storey upgrading, Pushover analysis, Seismic behavior

1. INTRODUCTION

Masonry construction is common, and it has gained popularity mainly due to its low cost, widespread geographical availability, thermal insulation, protection from fire, durability, low maintenance cost, and it is easy to construct. Masonry has good compressive strength, thus the structures will behave well as long as the loads are vertical, but when a horizontal inertial earthquake forces act, they start to develop shear and flexural stresses. Masonry is a non-homogeneous, non-isotropic material, with a mechanical behavior dominated by the non-linear phase, characterized by negligible strength and brittleness in tension, and dissipative with softening behavior in compression. To increase the number of standardized economic solutions of masonry structures, further research is necessary into the problems that may occur during their construction and exploit. At the same time, based on the previous facts, it is necessary to consider masonry structures as vulnerable to earthquakes[1].

An assessment of the seismic vulnerability of masonry structures is a complex task that must be performed by engineers. Therefore, it is necessary to make a balance between sufficient accuracy and simplicity and availability of the

assessment for frequent use in practice. For this purpose, it is essential to know the characteristics of the structure being designed and the relevant actions on it, as well as the properties of the materials that will be used for construction. All the unreliability of the assessment and input data can create unfavorable solutions and lead to undesirable consequences [2].

The regulations for the design of masonry structures under static and dynamic actions in Serbia have been significantly improved with the introduction of Eurocodes. An assessment of the seismic resistance of the common masonry structures is conducted in accordance with provisions from the regulation: SRPS EN 1996-1-1 [3], SRPS EN 1998-1 [4], SRPS EN 1998-1/NA [5], and SRPS EN 1998-3 [6].

The seismic vulnerability of masonry structures is rarely assessed by linear elastic analysis procedures. Non-linear dynamic analysis methods represent the most reliable tool. Nevertheless, they are very complex and require a great amount of computational resources and time, and further research efforts are still needed before they can be confidently used in standard design. Therefore, pushover procedures have been increasingly recognized as effective tools in seismic design and vulnerability assessment: they provide information on both the strength and ductility of the structure while preserving the simplicity of static analysis. Here a single degree of freedom (SDOF) system was derived to represent the multi-degree of freedom (MDOF) structure via an equivalent or "substitute" structure. However, the simplicity of these procedures is paid with a series of limitations that may restrict their application only to some classes of structures. The main outcome of pushover procedures is the curve relating the displacement of a certain controlling point to the resultant of a predefined horizontal distributed force applied to the structure. This curve, representing the seismic capacity of the structure, is then compared with the seismic demand, expressed in terms of response spectrum [7, 8].

Two basic things define different pushover procedures, one being the choice of the load pattern and the second simplification model of the pushover curve for design purposes. In pushover procedures the magnitude of structural loading is incrementally increased following a certain predefined pattern, thus causing weak links and developing failure modes. Pushover analysis is basically an attempt to evaluate the real seismic capacity of the structure, and it is effective for performance-based design. A drawback of the method is that for masonry structures, until now, the best pattern of loads is not yet determined. Additionally, it gives a time-independent displacement shape. The advantage of this procedure is that it is able to locate the most vulnerable parts of the structure [8].

The use of an equivalent static, simplified non-linear (pushover) method for seismic assessment of masonry structures was introduced in 1978 by Tomaževic(SFR Yugoslavia, today Republic of Slovenia) [9]. Such a method has undergone several refinements through the years and firstly was formulated anInvariant-force Pushover Analysis (IPA).This method considered that pushover analyses with invariant lateral force distribution cannot detect changes caused in non-linear dynamic characteristics due to the evolution of damage in the structure. More advanced pushover analysis like Modal Pushover Analysis (MPA) was developed based on lumped mass systems like frame structures. Unlike previous methods,the MPA permits the consideration of higher modes in pushover analysis and asymmetrical structures in the layout plan. One of the limitations of this method is that the sequence of damage development cannot be directly controlled, since the final deformed shape can be represented only by the superposition of the deformed shapes from each mode. Almost at the same time as the MPA, Adaptive Pushover Analysis (APA) was developed. The APA can represent the development of the damage during the analysis by updating the lateral force distribution pattern as damage propagates. This method considers inelasticity at the current step and updates the lateral load distribution accordingly. SRPS EN1998-1 suggests the application of the N2 method, based on the combination of pushover analysis with the capacity spectrum approach. The N2 method correlates the displacement capacity of the structure to the displacement demand of the expected earthquake. At first, the method was introduced for symmetrical structures, for which good performance was observed. Additionally, over time, the N2 method has extended to asymmetrical frame structures, structures irregular in layout plan, and structures irregular both in plan and height. The N2 introduced the impact of torsion with higher modes as well, and is relatively easy to use, thus it is more economical in relation to the use of non-linear dynamic analysis[10-12].

It has been observed that under the action of moderate to severe earthquakes the masonry structures performed the worst, causing the largest loss of lives as well as properties. Thus, to save the people from the collapse of such buildings during an earthquake it is required to make them earthquake resistant. For existing buildings, seismic vulnerability evaluation is needed, along with possible retrofitting [13]. Also, with an increase of population in cities, there is a constant need for new residential spaces. As a more economical solution than the construction of new buildings, upgrading existing buildings by adding one or more floor levels is often conducted. Such new structures must meet the same seismic resistance regulations as the existing ones. On the other hand, there are currently insufficient guidelines for modelling uncommon masonry structural configurations [2]. For these purposes, researchers are evaluating different types of masonry structures that require retrofitting and upgrading. By using pushover analysis, Manojlović et al. showed the possibilities of seismic retrofitting and upgrading an existing grammar school masonry building in Novi Sad, Serbia [14]. Galasco et al. showed the three-dimensional model of an old masonry building assembled with frame-type macro-element models of the walls and orthotropic membrane elements to represent the mechanical

behavior of flexible timber floors. This modelling approach, although very effective in representing the actual behavior, does not allow to use of common simplifications such as rigid floor motion [15]. Ademović et al. discussed the behavior of a typical masonry building in Bosnia and Herzegovina built in the 1950s without any seismic guidelines [8]. Bocciarelli and Barbieri proposed a numerical procedure for pushover analysis of an old masonry tower with displacement control [1].A similar discussion was provided by Shehu[16]. Giordano et al. investigated the seismic response of plan irregular (asymmetric) two-storey masonry building structure to evaluate the magnitude of torsional coupling and the applicability of 3D pushover analysis for assessing the behavior under earthquakes[17].

This paper shows a comparative study for upgrading of existing residential two-storey masonry building by adding one additional floor level on four proposed models. The results of pushover analyses performed on proposed models were evaluated with the respect to the regulations. In the computations, two different lateral load distributions were assumed since the appropriate lateral loads profile is not always obvious. Based on various considered modelling approaches, different responses of the structures were identified.

2. PUSHOVER ANALYSIS ACCORDING TO EUROCODE 8-1

According to SRPS EN 1998-1, a pushover analysis must be performed with two lateral load patterns. A load distribution corresponds to the fundamental mode shape and a uniform distribution proportional to storey masses. Classical steps of the pushover analysis are:

- Modelling of the structure with concentrated storey masses with elastic behavior.
- Determination of the fundamental period of vibration.
- Determination of the fundamental mode shape (Eigen vectors).
- Determination of the modal mass coefficient for the first natural mode.
- Determination of the lateral displacements at each level for the first natural mode.
- Determination of seismic forces at each level for the first natural mode.
- Transformation of the MDOF system to an equivalent SDOF with an equivalent mass m^* as formulated in (1).

$$m^* = \sum m_i \cdot \Phi_i = \sum \bar{F}_i \tag{1}$$

- Determination of the modal participation factor of the first natural mode according to (2).

$$\Gamma = \frac{m^*}{\sum m_i \cdot \Phi_i^{\,2}} = \frac{\sum \bar{F}_i}{\sum \left(\frac{\bar{F}_i^2}{m_i} \right)} \tag{2}$$

- Determination of the force F^* and the displacement d^* of the equivalent SDOF represented in eq. (3, 4).

$$F^* = \frac{F_b}{\Gamma} \tag{3}$$

$$d^* = \frac{d_n}{\Gamma} \tag{4}$$

In (3, 4) F_b is the base shear force and d_n the control node displacement of the MDOF system.

- Determination of the idealized bilinear force-displacement relationship as shown in Figure 1. The yield force F_y^*, which represents also the ultimate strength of the equivalent SDOF system, is equal to the base shear force at the formation of the plastic mechanism. The initial stiffness of the equivalent SDOF system is determined in such a way that the areas under the actual and the equivalent SDOF system force displacement curves are equal. Based on this assumption, the yield displacement of the equivalent SDOF system d_y^* is given in (5).

$$d_y^* = 2 \cdot \left(d_m^* - \frac{E_m^*}{F_y^*} \right) \tag{5}$$

In (5) E_m^* is the actual deformation energy up to the formation of the plastic mechanism. Figure 1 shows the principle of energy idealization.

- Determination of the period of the equivalent SDOF system T^* as in (6).

$$T^* = 2 \cdot \pi \cdot \sqrt{\frac{m^* \cdot d_y^*}{F_y^*}} \tag{6}$$

- Determination of the target displacement for the equivalent SDOF system is given in (7).

$$d_{et}^{*} = S_e\left(T^{*}\right) \cdot \left(\frac{T^{*}}{2 \cdot \pi}\right)^2 \tag{7}$$

$S_e\left(T^{*}\right)$ is the elastic acceleration response spectrum at the period T^{*}. Determination of the target displacement d_t^{*} for structures in the short period range is formulated in (8) for the elastic response and (9) for the non-linear response, while $T^{*} < T_c$. For structures in the medium and long period ranges, target displacement is given in (10), while $T^{*} \geq T_c$. q_u is the ratio between the acceleration in the structure with unlimited elastic behavior $S_e\left(T^{*}\right)$ and in the structure with limited strength F_y^{*} / m^{*}. T_c is the border between short and medium vibration periods.

$$If \frac{F_y^{*}}{m^{*}} \geq S_e\left(T^{*}\right) \rightarrow d_t^{*} = d_{et}^{*} \tag{8}$$

$$If \frac{F_y^{*}}{m^{*}} < S_e\left(T^{*}\right) \rightarrow d_t^{*} = \frac{d_{et}^{*}}{q_u} \cdot \left(1 + \left(q_u - 1\right) \cdot \frac{T_c}{T^{*}}\right) \geq d_{et}^{*};\ q_u = \frac{S_e\left(T^{*}\right) \cdot m^{*}}{F_y^{*}} \tag{9}$$

$$d_t^{*} = d_{et}^{*} \tag{10}$$

- The target displacement of the MDOF system is presented in (11).

$$d_t = \Gamma \cdot d_t^{*} \tag{11}$$

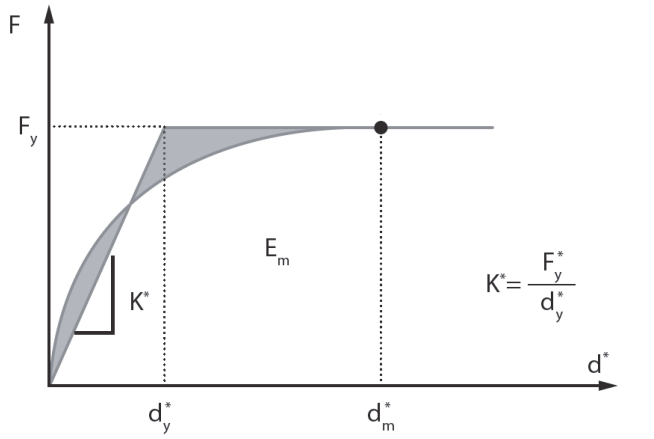

Figure 1: Linearization of the capacity curve[18]

3. CASE STUDY

To evaluate the most suitable structural solution, in terms of seismic vulnerability, for the upgrade of an existing residential two-storey masonry building, four different models of upgrading were made and their responses were observed, as well as the behavior of the existing building. Characteristic floor layout and three-dimensional representations of models are shown in Figure 2 and marked as:

- M0 - model of the structure of the existing building, as an unreinforced masonry building, with the found mechanical and geometric characteristics of load-bearing structural elements.
- M1 - model of the structure of the upgraded existing building with an additional floor modelled like the lower floors (unreinforced masonry), only with horizontal confining elements along the edges of the slabs, without vertical confining elements.
- M2 - model of the structure of the upgraded existing building with an additional floor modelled like confined masonry with horizontal confining elements along the edges of the slabs and vertical confining elements at the ends and crossings of the walls and at appropriate distances, while lower floors remain unchanged like unreinforced masonry.
- M3 - model of the structure of the upgraded existing building with an additional floor modelled like confined masonry with horizontal confining elements along the edges of the slabs and vertical confining elements that extend from the foundation to the top of the building only on the shorter façade walls of the building.

- M4 - model of the structure of the upgraded existing building with an additional floor modelled like confined masonry with horizontal confining elements along the edges of the slabs and vertical confining elements that extend from the foundation to the top of the building located in characteristic places on all façade walls of the building.

For modelling of the building structure and proposed upgraded solutions, the software AmQuake was used with the finite element method for numerical calculation and common macro elements. Additionally, the software used the equivalent frame approach for the pushover analysis which considers all modelled line structural elements with their inelastic behavior. All models have openings in walls in accordance with architectural design, and around them software generated new line macro elements for parapets and spandrels. The assumption of rigid floor motion was introduced in all models. The AmQuake uses pushover analysis and determines the target displacements in accordance with the provisions of regulations [19]. The obtained target displacements were compared with the corresponding capacities.

Although SRPS EN 1998-1 requires the use of mean values of the material properties, in this study the characteristic values were used, which provided a certain safety to the results of the pushover analysis. In the analysis, the stiffness of cracked sections was taken as half of the stiffness value of uncracked sections. Soil type C, acceleration a_{gR}= a_g= 0.20g,and building importance class II represented the seismic input. As SRPS EN 1998-1demands, two different load patterns of the seismic force were applied to all models for the pushover analysis, triangular and uniformly distributed lateral force in positive directions of the X and Y axis[4]. Additionally, in both these directions were added eccentricities equal to +0.05 times the building dimension in the plane perpendicular to the direction of the seismic force for the purpose of creating accidental torsional effects.

Pushover analysis was conducted with consideration of the ultimate limit state (ULS) and damage limitation state (DLS). By SRPS EN 1998-3, for the masonry and reinforced concrete elements were taken drift limit for bending failure equal to 0.008 and drift limit for shear failure equal to 0.004[6]. The analysis included only the stiffness of the load-bearing walls, while the stiffness of the partition walls was not taken into account, only their mass.

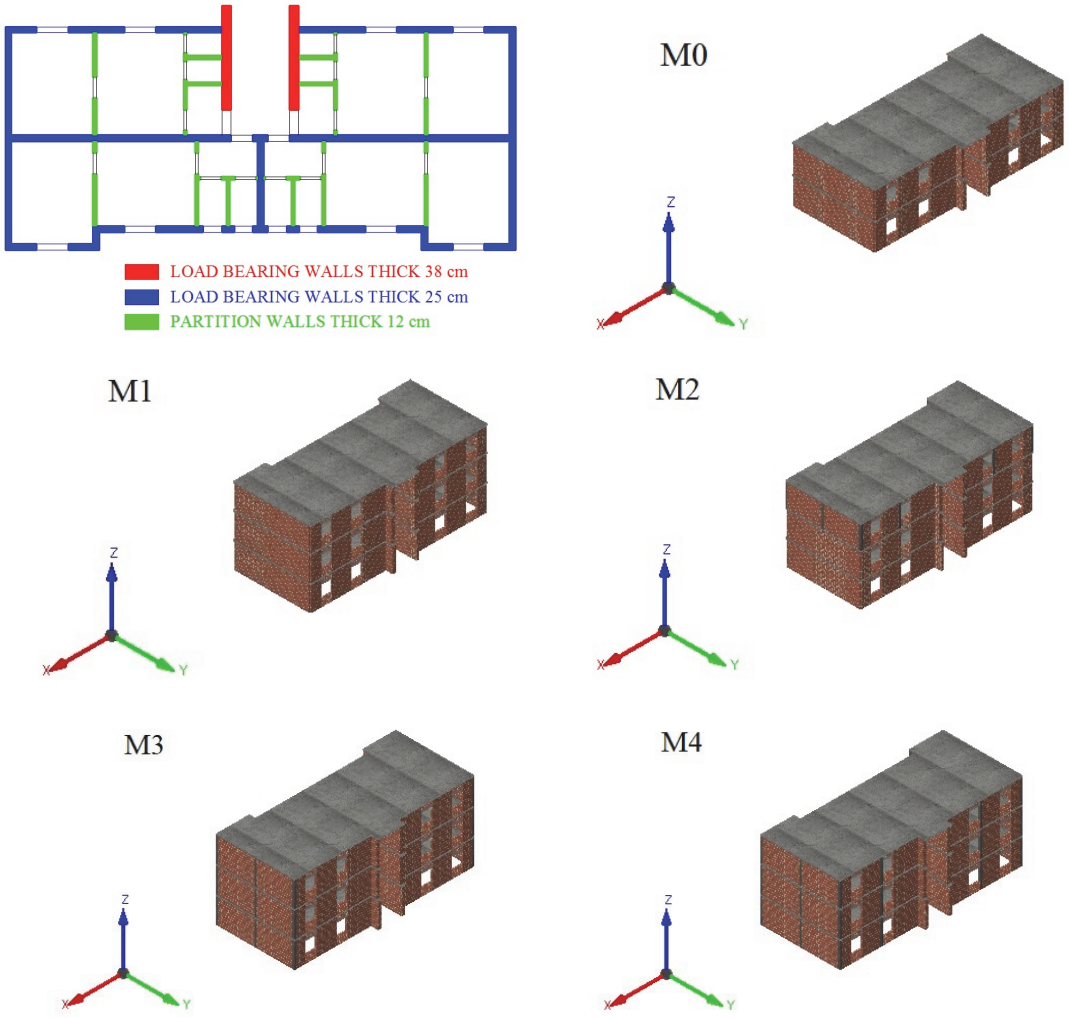

Figure 2: Characteristic floor layout and three-dimensional representations of models for the existing building M0, and upgrading solutions M1-4

3.1. Materials and loads of the existing building

Representing masonry building is situated in Serbia and it is relatively new. It consists of a high ground floor and one upper floor, with a gross floor area of 199.55 m^2 and a characteristic floor layout as shown in Figure 2. Each floor level consists of four residential units with similar gross areas. Vertical communication inside the building is provided by the central staircase area. Storey height is equal to 300 cm and the clear height is equal to 280 cm. Structural walls were constructed using clay blocks without reinforcement, and floor slabs were made with reinforced concrete (RC). During inspections of building design data, no vertical confining elements were observed, only horizontal confining RC elements were found at floor levels and lintels made with reinforced concrete.

The façade walls of the building are with a thickness of 25 cm as internal load-bearing walls. The walls around the staircase are with a thickness of 38 cm and the partition walls are 12 cm thick. All walls are made of porotherm clay blocks and dry-fix mort. Characteristic compressive strength calculated based on SRPS EN 1996-1-1 is f_k = 3.87 MPa for bearing walls thickness of 25 and 38 cm. Characteristic initial shear strength of masonry under zero compressive stress was adopted asf_{vk0}= 0.30 MPa, whereas for the limit value of characteristic masonry shear strength f_{vlt} =0.52 MPa was used. Furthermore, the short-term secant modulus of elasticity of masonry was determined as $E = 1000 \cdot f_k$ = 3.869GPa. For the shear modulus of masonry, a calculated value of G =1.548GPa was adopted. Horizontal confining elements and lintels were made with concrete class C16/20 (f_{ck}= 16 MPa) along with reinforcement B500 (f_{yk}= 500 MPa). Concrete elements have a rectangular cross-section of 25/20 cm, and they are reinforced with four 12 mm diameter longitudinal bars and 6 mm diameter stirrups spaced at 15 cm. Solid concrete slabs are designed on all floor levels, including the roof.

The existing building was designed with self-weight applied to every floor structure amounted to 4.0 kN/m^2, an additional dead load applied at floors amounted to 1.5 kN/m^2, and applied variable load at the floor (except the roof) amounted to 2.5 kN/m^2.The roof floor structure was designed with self-weight, additional dead load, and the snow load equal to 5.0 kN/m^2, 0.5 kN/m^2, and 1.0 kN/m^2, respectively.

3.2. Materials and loads of the upgraded floor level

To upgrade the existing building, the considered models used walls with the same mechanical and geometric characteristics as the walls on the lower floors. All added RC structural elements are designed from concrete classC25/30 (f_{ck}= 25 MPa). Along the edges of the slabs, horizontal confining elements with a rectangular cross-section of 25/20 cm were designed and reinforced with four 14 mm diameter longitudinal bars and 6 mm diameter stirrups spaced at 15 cm. The lintels have the same characteristics as the horizontal confining elements. Vertical confining elements were designed with a square cross-section of 25/25 cm at the ends and crossings of the walls and at appropriate distances. They were also reinforced with four 14 mm diameter longitudinal bars and 6 mm diameter stirrups spaced at 15 cm.

The additional floor level was designed with a new RC roof slab and with applied self-weight, self-weight of the roof structure, additional dead load, and the snow load to 3.0 kN/m^2, 2.5 kN/m^2, 0.5 kN/m^2, and 1.0 kN/m^2, respectively.

4. RESULTS OF THE STUDY

Pushover analysis was performed with both types of elastic spectrum. This paper shows only results of the analysis with type 1 spectrum, as authoritative for the given soil acceleration. For target displacements, the N2 method was used as part of regulations in the software AmQuake[19]. Tables 1-2 show the most important parameters of the analysis for the uniform and the triangular distributions of the seismic force in X and Y positive directions: yield force (F_y) of the idealized bilinear pushover curve for the MDOF system, target top floor displacements for the ULS ($d_{t,ULS}$) and DLS ($d_{t,DLS}$), the ULS (d_t) and DLS ($d_{c,DLS}$) capacities for the top floor displacements, calculated maximum inter-storey drift (*RShift*), DLS inter-storey drift criterion (*RShift* criterion), period of vibration of the idealized structural system with SDOF (T^*), capacity ductility factor μ and yield displacement (d_y) of the idealized bilinear pushover curve for the MDOF system.

Table 1: Most important results of the pushover analysis for building models with uniform distributed load

Model	M0		M1		M2		M3		M4	
Direction	+X	+Y	+X	+Y	+X	+Y	+X	+Y	+X	+Y
F_y[kN]	1644.44	1503.91	1721.32	1380.19	2073.71	2249.21	1776.05	2493.19	2072.77	2553.65
$d_{t,DLS}$[mm]	1.278	1.105	3.600	2.766	1.745	1.715	3.909	2.881	4.230	2.872
$d_{c,DLS}$[mm]	4.956	5.097	15.597	17.197	7.600	6.601	16.412	10.390	15.400	10.564
$d_{t,ULS}$[mm]	4.894	4.928	17.925	16.839	7.399	6.230	18.755	10.313	17.843	9.951
d_t[mm]	4.956	5.097	15.372	17.197	7.600	6.601	15.812	10.390	14.600	10.564
RShift	0.0009	0.0013	0.0044	0.0032	0.0020	0.0015	0.0041	0.0020	0.0044	0.0022
RShift criterion	0.177	0.259	0.872	0.642	0.392	0.309	0.822	0.394	0.876	0.431

T^*[s]	0.140	0.133	0.217	0.192	0.161	0.160	0.226	0.196	0.234	0.195
μ	2.118	2.674	3.402	6.032	2.568	2.084	3.174	1.989	2.334	1.987
d_y[mm]	2.340	1.906	4.518	2.851	2.960	3.168	4.982	5.223	6.256	5.317

Table 2: Most important results of the pushover analysis for building models with triangular load

Model	M0		M1		M2		M3		M4	
Direction	+X	+Y	+X	+Y	+X	+Y	+X	+Y	+X	+Y
F_y[kN]	1231.14	1165.31	1311.20	1046.49	1910.89	2010.59	1319.58	2118.42	2047.59	2203.59
$d_{t,DLS}$[mm]	0.942	1.071	4.447	8.030	2.442	2.063	4.313	3.173	4.733	3.089
$d_{c,DLS}$[mm]	4.337	6.097	15.542	20.192	10.462	7.759	21.018	12.190	19.072	11.425
$d_{t,ULS}$[mm]	4.179	5.741	24.005	34.250	10.323	7.677	23.628	12.130	18.632	11.341
d_t[mm]	4.337	6.097	15.392	20.042	10.462	7.759	20.773	12.190	19.072	11.425
RShift	0.0011	0.0017	0.0040	0.0040	0.0024	0.0016	0.0041	0.0021	0.0033	0.0019
RShift criterion	0.224	0.336	0.800	0.789	0.488	0.318	0.810	0.413	0.658	0.387
T^*[s]	0.120	0.127	0.223	0.275	0.172	0.161	0.218	0.190	0.230	0.189
μ	2.617	3.608	3.274	3.504	2.565	2.063	4.565	2.201	2.500	2.061
d_y[mm]	1.657	1.690	4.702	5.720	4.078	3.761	4.550	5.538	7.630	5.543

According to the presented results, two models meet the ULS criteria, the model of the existing building M0 and the combined model of the upgraded building M2 where the lower floors are left with unreinforced masonry (URM) and the added floor contains horizontal and vertical confining elements (CM). In the case of the DLS criteria, it was found to be irrelevant for the proposed models, as all target parameters meet the criteria.

Yield force (F_y) is larger in the X direction under uniform load for the URM models M0 and M1, while for the models M2-4 with CM yield force is larger in the Y direction under triangular load. The smallest difference in the magnitude of the horizontal seismic force when the load is uniform or triangular is for M2 which is the only model of upgrading that meet ULS criteria, while the largest difference between the horizontal forces occurs on M3.

From Figures 3-7 it can be seen that for all models except M1 the DLS displacements ($d_{t,DLS}$) are always on the parts of the pushover curves corresponding to the linear elastic structural response, which is an expected result. Only for model M1 $d_{t,DLS}$ was observed on part of the pushover curve related to the non-linear response.

The most critical parameter of the analysis is ULS top floor displacement ($d_{t,ULS}$) that can be expected for the given structure and seismic demand, and it must be smaller than top floor displacement when the structure starts to collapse (d_t) or when the base shear force drops below 80% of its maximal value. As stated, this criteria was met only by two models, M0 and M2. In terms of safety margin for the ULS criteria, defined as the percentile ratio between the target and the capacity values as presented in (12), model M1 performed with the lowest safety of -70,89% for Y direction and triangular load, then models M4, M3, M2, M0 with their the most unfavourable safety of -22,21% (X, uniform load), -18,61% (X, uniform load), 1,05% (Y, triangular load), 1,25% (Y, triangular load), respectively. These, the most unfavourable displacements for each model are shown in Figures 3-7 with the pushover force-displacement curve and idealized bilinear force-displacement diagram. For URM model M1 it is expected to perform the worst in terms of displacements in the Y direction which is shorter and has less stiffness and under a triangular load pattern that accumulates higher top floor displacements. Similar behavior showed model M2 which has only vertical confining elements on top floor level and lower levels are URM, thus it has an increase in stiffness, decrease in inter-storey drift, and overall displacements values. Different behavior showed models M3-4 with vertical confining elements from the top floor to the foundation on the façade, and they performed the worst in the X direction under a uniform load pattern, thus indicating the formation of hinges in the vertical confining elements. This change in unfavourable conditions is probably due to inserted vertical confining elements increasing more stiffness in the Y than X direction.

$$ULS\ safety\ margin = \frac{d_t - d_{t,ULS}}{d_t} \cdot 100\% \tag{12}$$

RShift presents calculated maximum inter-storey drift from all storey's *deflection/storey height* and it is compared with DLS inter-storey drift criterion (*Rshift/Damage limit*). For three-storey models, the highest *RShift* has URM model M1. The introduction of vertical confining elements from the top floor to the foundation on the façade had lowered *RShift*, but only significantly in a shorter Y direction. Combined model M2 performed the best in terms of inter-storey drift. This may be due to the fact that in SRPS EN 1998-3 the same values of drift limits apply for all masonry structures, even though they are explicitly defined for the URM ones.

Periods of vibration of the idealized structural system with SDOF (T^*) for proposed models are similar for different directions and higher in the longer X direction as expected, only M2 with triangular load is an exception. All periods have lower values than period with constant acceleration in the elastic response spectrum (T_c = 0.6 s for soil type C), thus all models are in the short period range.

Capacity ductility factor μ for ULS is determined as the ratio between capacity displacement (d_t) and yield displacement (d_y), and given values in tables 1-2 were calculated manually since AmQuake provides target ductility factor values calculated with target displacement. For models M0 and M2 that meet the ULS criteria with high non-linear response, there is a low ductility reserve which makes these models sensitive to seismic action, as shown on Figures 3 and 5.

On the left side of Figures 3-7 is shown the deformation of models with damage factor *CF* (confidence factor), which is a parameter indicating how much the element response deviates from the elastic one. It ranges from 0 for the fully undamaged to 1 for the fully damaged conditions.

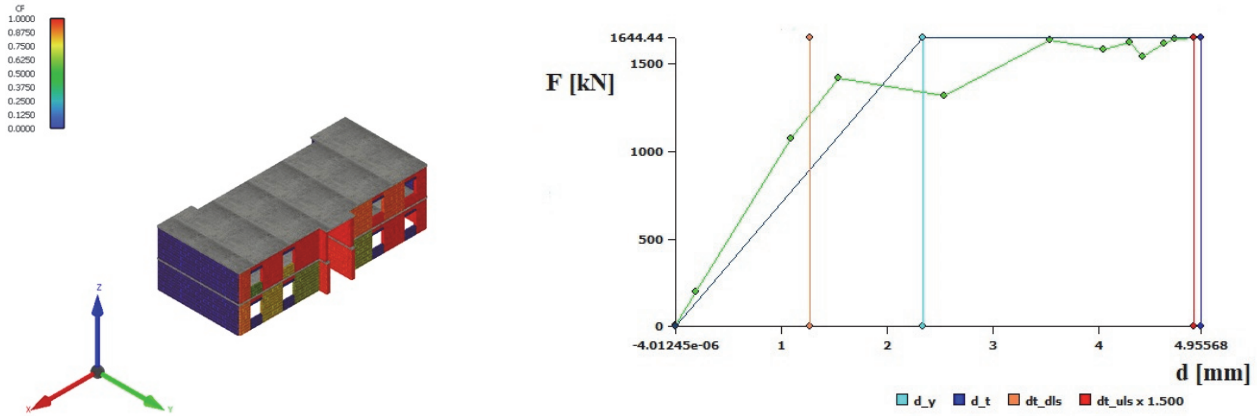

Figure 3: (left) Damage factor *CF*, (right) pushover force-displacement curve with idealized bilinear force-displacement diagram for the model M0, +X direction and uniformly distributed load

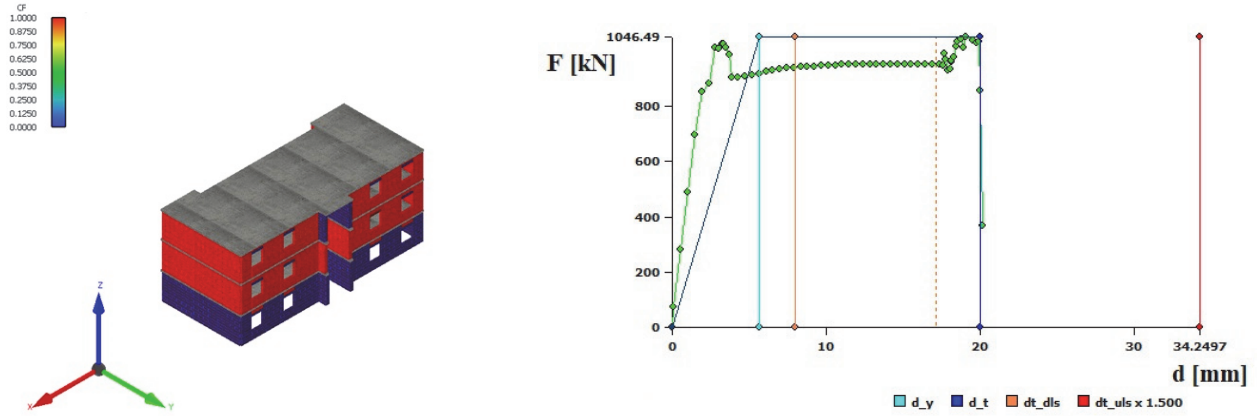

Figure 4: (left) Damage factor *CF*, (right) pushover force-displacement curve with idealized bilinear force-displacement diagram for the model M1, +Y direction and triangular load

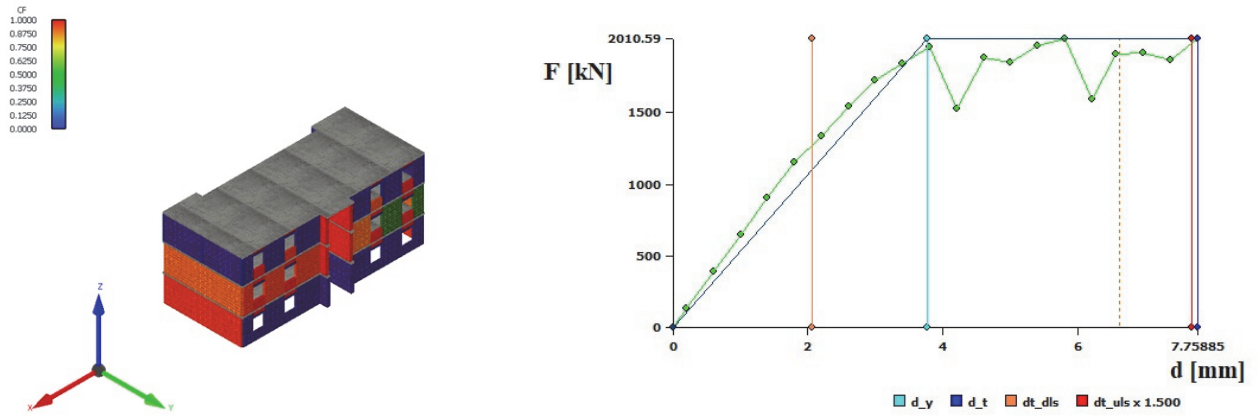

Figure 5: (left) Damage factor *CF*, (right) pushover force-displacement curve with idealized bilinear force-displacement diagram for the model M2, +Y direction and triangular load

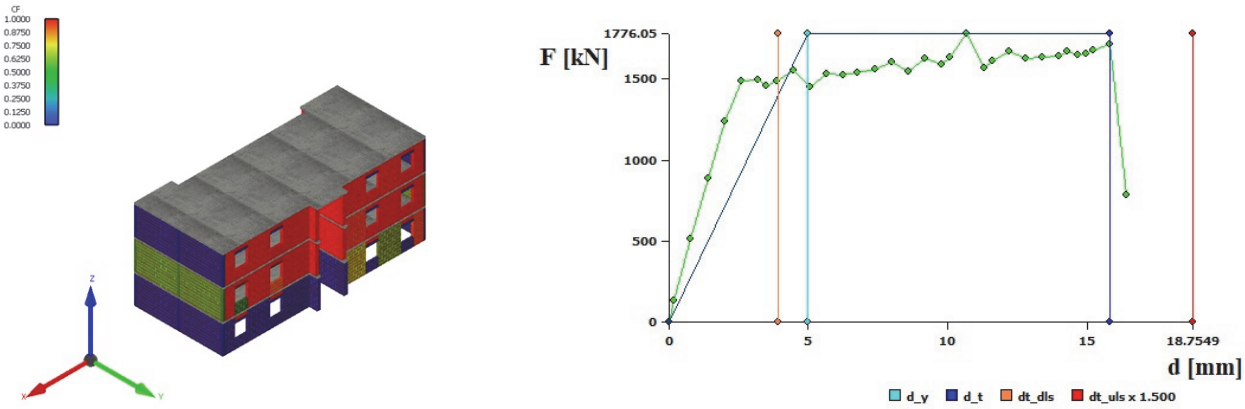

Figure 6: (left) Damage factor *CF*, (right) pushover force-displacement curve with idealized bilinear force-displacement diagram for the model M3, +X direction and uniformly distributed load

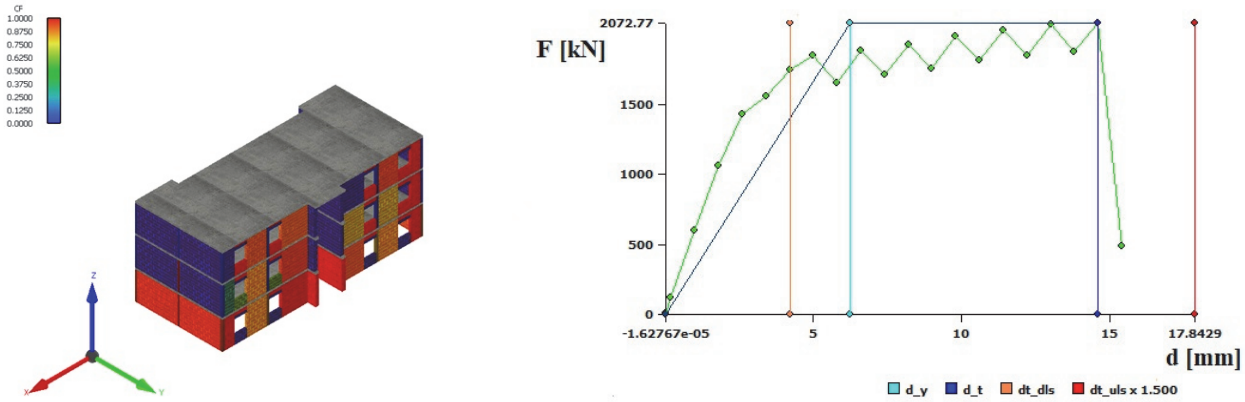

Figure 7: (left) Damage factor *CF*, (right) pushover force-displacement curve with idealized bilinear force-displacement diagram for the model M4, +X direction and uniformly distributed load

5. CONCLUSIONS

In this paper the seismic vulnerability of an existing two-story unreinforced masonry building was analyzed, and models for its upgrade with another floor level were proposed, by using pushover analysis. The existing building showed good properties for the effect of horizontal forces from earthquakes. It was analyzed four upgraded models of existing building:

1. model without vertical confining elements,
2. model with vertical confining elements only in the added floor level,
3. model with vertical confining elements along the shorter façade walls and along the entire height of the building,
4. model with vertical confining elements along the entire height of the building along all façade walls.

The ULS parameters from earthquake using pushover analysis, was satisfied only by a second model with vertical confining elements only in the added floor level. The model without vertical confining elements performed the worst.

Current regulations demand the use of two different lateral load patterns in pushover analysis without a detailed explanation of each pattern's purpose. This paper confirmed that, as during analysis models showed different behaviors with uniformly distributed or triangular loads depending on proposed confining. While using software AmQuake for pushover analysis capacity ductility factor should be calculated manually.

Seismic response of structure is in a tight connection with confining, and it has beneficial effects especially in a case of the shear capacity. Positioning of confining elements has a key role for evaluation of seismic vulnerability, and ductility capacity of the masonry structures. Further research on this topic must include models with retrofitting solutions that are more common in practice, such as strengthening of the existing walls or installing vertical confining elements along the entire height of the building and in all load-bearing walls. There is a need for guiding the engineers toward proper and better modelling of masonry structures.

REFERENCES

[1] M. Bocciarelli and G. Barbieri, "A numerical procedure for the pushover analysis of masonry towers", Soil Dynamics and Earthquake Engineering, Vol. 93, pp. 163-171, http://dx.doi.org/10.1016/j.soildyn.2016.07.022, (2017)

[2] D. Manojlović, Đ. Jovanović and V. Vukobratović, "Pushover analysis of a four-storey masonry building designed according to Eurocode", Proceedings of International Conference "iNDiS 2018", Novi Sad (Serbia), 21-23 November 2018, pp. 547-554, (2018)

[3] SRPS EN 1996-1-1: 2016, Design of masonry structures - Part 1-1: General rules for reinforced and unreinforced masonry structures, Institute for standardization of Serbia, Belgrade, (2016)

[4] SRPS EN 1998-1: 2015, Design of structures for earthquake resistance - Part 1: General rules, seismic actions and rules for buildings, Institute for standardization of Serbia, Belgrade, (2018)

[5] SRPS EN 1998-1/NA: 2015, Design of structures for earthquake resistance - Part 1: General rules, seismic actions and rules for buildings. - National Annex, Institute for standardization of Serbia, Belgrade, (2018)

[6] SRPS EN 1998-3: 2015, Design of structures for earthquake resistance - Part 3: Assessment and retrofitting of buildings, Institute for standardization of Serbia, Belgrade, (2015)

[7] G. Magenes, "A method for pushover analysis in seismic assessment of masonry buildings", Proceedings of International Conference "12 WCEE 2000", Auckland (New Zeland), 30 January - 4 February 2000, p. 1866, (2000)

[8] N. Ademović, M. Hrasnica and D. V. Oliveira, "Pushover analysis and failure pattern of a typical masonry residential building in Bosnia and Herzegovina", Engineering Structures, Vol. 50, pp. 13-29, http://dx.doi.org/10.1016/j.engstruct.2012.11.031, (2013)

[9] M. Tomaževic, "The computer program POR", Report ZRMK, (1978)

[10] Y. Endo, L. Pela and P. Roca, "Review of different pushover analysis methods applied to masonry buildings and comparison with nonlinear dynamic analysis", Journal of Earthquake Engineering, Vol. 21 (8), pp. 1234-1255, https://doi.org/10.1080/13632469.2016.1210055, (2016)

[11] A. Rooshenas, "Comparing pushover methods for irregular high-rise structures, partially infilled with masonry panels", Structures, Vol. 28, pp. 337-353, https://doi.org/10.1016/j.istruc.2020.08.073, (2020)

[12] H. Azizi-Bondarabadi, N. Mendes and P. B. Lourenço, "Higher mode effects in pushover analysis of irregular masonry buildings", Journal of Earthquake Engineering, Vol. 25 (8), pp. 1459-1493, https://doi.org/10.1080/13632469.2019.1579770, (2019)

[13] T. M. Ferreira, N. Mendes and R. Silva, "Multiscale seismic vulnerability assessment and retrofit of existing masonry buildings", Buildings, Vol. 9 (4), p. 91, https://doi.org/10.3390/buildings9040091, (2019)

[14] D. Manojlović, Đ. Lađinović and V. Vukobratović, "Seismic retrofit of an existing grammar school masonry building", Proceedings of International Conference "1CroCEE", Zagreb (Croatia), 22-24 March 2021, pp. 899-908, https://doi.org/10.5592/CO/1CroCEE.2021.23, (2021)

[15] A. Galasco, S. Lagomarsino and A. Penna, "On the use of pushover analysis for existing masonry buildings", Proceedings of International Conference "1st ECEES", Geneva (Switzerland), 3-8 September 2006, p. 1080, (2006)

[16] R. Shehu, "Implementation of pushover analysis for seismic assessment of masonry towers: Issues and practical recommendations", Buildings, Vol. 11 (2), p. 71, https://doi.org/10.3390/buildings11020071, (2021)

[17] A. Giordano, M. Guadagnuolo and G. Faella, "Pushover analysis of plan irregular masonry buildings", Proceedings of International Conference "14WCEE", Beijing (China), 12-17 October 2008, (2008)

[18] M. Youcef, K. Abderrahmane and C. Benazouz, "Seismic performance of RC building using spectrum response and pushover analyses", International Congress and Exhibition "Sustainable Civil Infrastructures: Innovative Infrastructure Geotechnology", Sharm Elsheikh (Egypt), 15-19 July 2017, pp. 158-169, http://dx.doi.org/10.1007/978-3-319-61914-9_13, (2018)

[19] B. Milošević, "AmQuake: Statička i dinamička analiza zidanih konstrukcija", Faculty of Mechanical and Civil Engineering, Kraljevo (Serbia), ISBN: 978-86-6090-058-8, (2022)

ORIGINAL SCIENTIFIC PAPER OPEN ACCESS

Microstructural analysis of a HP 40Nb alloy aged

Milica Timotijević[1], Olivera Erić Cekić[1,2*], Dragan Rajnović[3], Petar Janatović[3]

[1] University of Kragujevac, Faculty of Mechanical and Civil Engineering, Kraljevo, Serbia

[2] University of Belgrade, Innovation Center of Mechanical Engineering Faculty, Belgrade, Serbia

[3] University of Novi Sad, Faculty of Technical Science, Department of Production Engineering, Novi Sad, Serbia

ARTICLE INFO

* **Correspondence:** olivera66eric@gmail.com

DOI: 10.5937/engtoday2203041T

UDC: 621(497.11) **ISSN:** 2812-9474

Article history: Received 10 October 2022; Accepted 19 October 2022

ABSTRACT

In this paper, the change in the microstructure of the centrifugally cast heat-resistant alloys of HP40 Nb after exposure to 0.5h and 2h of ageing times at 1123K and 1323K were investigated. The microstructures of the as-received alloy and aged conditions were examined using light microscopy (LM) and scanning electron microscopy (SEM) equipped with an energy dispersive spectroscopy (EDS). The chemical composition of various phases and precipitates observed in the aged sample microstructure was characterized by the means of scanning electron microscopy SEM via back-scattered electron (BSE). The present results indicate that ageing enhanced the occurrence of different phenomena such as the transformation of primary M_7C_3 to $M_{23}C_6$ carbides and precipitation of secondary $M_{23}C_6$ carbides. It can be summarized that the present phases and the morphology of secondary carbides in the microstructure of aging results in higher values of hardness.

KEYWORDS

Heat resisting cast alloys, Aging, Microstructure, Carbides

1. INTRODUCTION

Thanks to the unique properties of centrifugally cast heat-resistant alloys of HP series, such as: high mechanical properties, corrosion resistance and stability of mechanical properties under service at temperatures below 1323K; these alloys are found in application in many industries such as petrochemical, chemical and commercial heat treating industries [1-8]. The centrifugally cast heat–resistant austenitic stainless steels are mostly used in petrochemical plants as alloys for production reformer tubes for hydrogen production by steam reforming [9-10].

The creep resistance of these alloys is high, thanks to the main alloying elements chromium and nickel, as well as other alloying elements (Ti, Zr, W and Cs) which in new generations of alloys have proven to be important for improving the required properties. Most heat-resistant alloys contain elements such as niobium, titanium, vanadium, and zirconium are commonly added to give higher creep resistance, as they form stable precipitates at the operating temperatures. In recent years, there has been growing interest in the application of the centrifugally cast HP40Nb alloy, which has been developed by adding a small amount of niobium element into HP40 alloy [11]. It should be mentioned that the addition of niobium in the HP alloy hinders the precipitation of chromium carbides and improves the mechanical properties (increase creep strength and creep ductility, as well as carburization resistance) [12].

The normal designed service life of reformer furnace tubes is defined by the API standard and is 100,000h [6, 7]. However, the actual working life varies from 30,000 to 180,000 h, because it is correlated with the damage mechanisms

(corrosion, fatigue, creep and erosion). In addition, the designed service life is not expected to be the same as the actual service life, because the actual operating conditions or the actual performance of the materials and components are not precisely known at the time of design.

It is known that the characteristic microstructure of as-cast HP alloys consists of an austenitic matrix strengthened by a network of intergranular eutectic-like primary chromium-rich carbides (M_7C_3 and/or $M_{23}C_6$ types (M= Cr, Ni, Fe) and niobium carbides of MC type (M= Nb) [13]. However, the microstructure of HP-modified steel of the catalyst tubes changes during service at elevated temperatures. It was reported in [14,15] that the microstructure of centrifugally cast Fe-Cr-Ni heat resistant alloys would change relatively rapidly during service at high temperatures, in a process known as microstructural steel ageing. During ageing, the primary chromium carbides eventually transform into $M_{23}C_6$; while intragranular secondary $M_{23}C_6$ carbides precipitate, also. As a result of this process, the original niobium carbides undergo an in situ phase transformation to a nickel-niobium silicate, $Ni_{16}Nb_7Si_6$ as reported by [16].

The purpose of the present study, due to the mentioned facts, is to examine the microstructural stability of the as cast tube made of HP 40Nb alloy after short-term exposure to temperatures of 1123K and 1323K for 0.5h and 2h, and to identify the types of phases and carbides in this alloy during ageing treatment.

2. EXPERIMENTAL PROCEDURE

2.1. Material

The material investigated in this work was machined out of one tube and manufactured of the centrifugally cast alloy HP-40Nb. The chemical composition of the studied material is shown in Table 1. The specimens were aged at 1123K and 1323K for 0.5h and 2 hours in the electric furnace in an air atmosphere and then each aged sample was cooled in air. The temperature was controlled by the thermocouple Pt-Pt13%Rh placed just above the sample. Microstructural observations were performed on samples of the as-cast tube before and after heat treatment. The chemical composition of various phases and precipitates observed was characterized by the means of scanning electron microscopy via back-scattered electron (BSE) imaging and EDS analyses.

2.2. Methods

Chemical composition

The chemical composition of the service reformer tube was analyzed through standard analytical spectrometry method, using the Optical Energy Spectrometer (OES) type I Spark 8860, Thermo Scientific, USA.

Metallurgical evaluation

Standard metallographic preparation techniques (mechanical grinding and polishing, followed by etching in Nital) were applied before light microscopy (LM) examinations on an Orthoplan microscope (Leitz, Germany).

Metallographic specimens were prepared in accordance with standard metallographic preparation technique: grinding (with SiC papers, from 180 to 2400), polishing (diamond suspensions with 6, 3, 1 and 1/4 μm particle size) and etched with a solution of 15 ml HCl, 10 ml Glycerol and 5 ml HNO_3.

The microstructure was examined using a scanning electron microscope JOEL JSM 6460 LV. The phases observed were analysed using an energy dispersive x-ray analyser system (EDS) INCA Oxford Instruments in conjunction with an SEM.

Hardness measurement

The Vickers hardness HV10 (ISO 6507) was determined with a test load of 98.07 N (10 kg) and a dwell time of 15 s. The testing machine was an HPO 250 (WPM, Germany).

3. ANALYSIS RESULTS AND DISCUSSION

3.1. Microstructure of as–cast material

The results of the chemical analysis of the investigated alloy are shown in Table 1. The results correspond to centrifugally cast alloy HP-40Nb.

Table 1: Chemical composition of the investigated alloy (in wt%)

	C	Si	Mn	Cr	Ni	Nb	Ti	Cu	Fe
Wt%	0.44	1.81	1.11	26.99	34.04	0.63	0.03	0.01	Bal.

3.2. Microstructural analysis (Light microscopy)

The microstructure of the as-cast samples consists of an austenite dendrite matrix, a cellular structure containing a network of skeleton shape eutectic primary carbides located at grain boundaries and between dendrites (Fig. 1a-b). At higher magnification observation, based on light contrast, the presence of two types of second phase particles of different morphology may be seen at the grain boundaries (Fig.1b). As can be seen in Fig.1b, one is a niobium-rich phase (white phase) having laminar type (or skeleton form) features, whereas the other is a chromium-rich phase (dark grey phase) having fine particle-like features [17, 18].

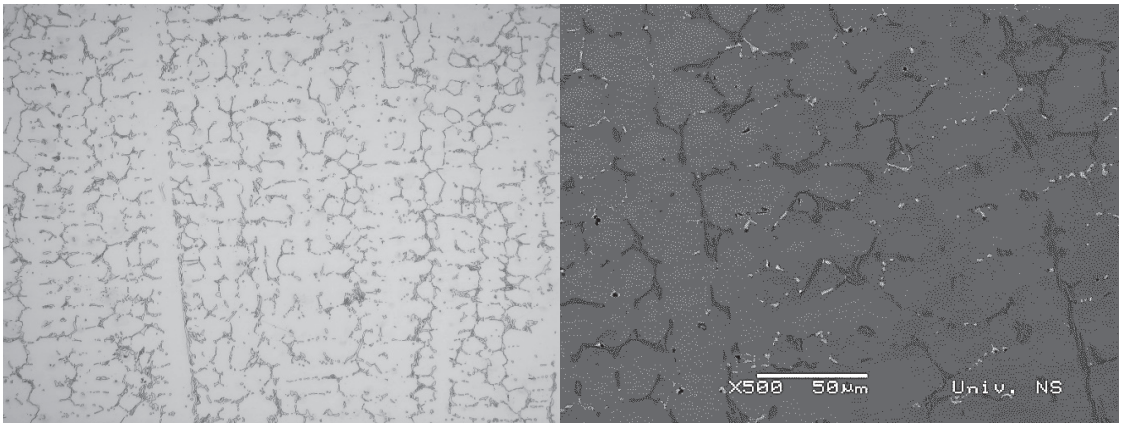

a) 100× b) 500×

Figure 1 Microstructure of HP40 Nb alloy as cast a) LM (Light microscopy) at low magnification (100×); b) SEM image at high magnification (500×).

3.3. Scanning Electron Microscopy (SEM) and X-ray Energy Dispersive Spectroscopy (EDS)

Figure 2a shows an SEM micrograph of the HP -40 Nb alloy in the as-cast condition. As seen in this Figure 2, the microstructure consists of an austenitic matrix and a network of primary carbides of two types: MC carbides (M = Nb, Ti) mainly NbC in white), and M_7C_3 carbides (M = Cr, Ni, Fe), in dark grey. One rich in Nb (bright particles in Fig.2a, Spec 3 and 4) and one rich in Cr (dark particles in Fig.2a, Spec 1, 2). Carbides in the inter-dendritic boundaries appear as lamellar or skeleton forms. The niobium-rich carbides are more stable at high temperatures compared to the secondary chromium carbides [12].

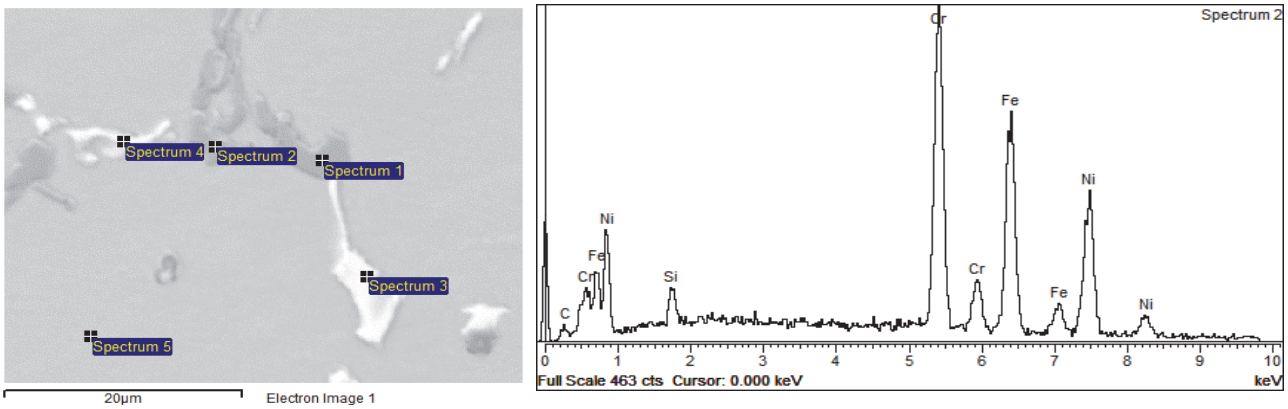

a) b)

Figure 2 Micrograph of present phases in as-cast HP40 Nb alloy: a) SEM micrographs (BSE), b) EDS spectrum of M_7C_3 carbide (M = Cr, Ni, Fe) in examination point 2 (Spectrum 2)

Table 2. Chemical composition (mass. %) of participate phases in HP40 Nb alloy, corresponding to Fig.2b

	C	Si	Cr	Mn	Ti	Fe	Ni	Nb
Spectrum 1	36.97		54.39			6.92	1.72	
Spectrum 2	15.83	3.41	28.73			27.11	24.93	
Spectrum 3	44.98		4.62		4.30	2.56	1.8	41.73
Spectrum 4	38.99	1.52	11.78		1.02	10.03	8.49	28.16

3.4. After ageing treatment

The change of microstructure during ageing at 1173K and 1323K after 0.5h and 2h is shown in Figure 3. The microstructures of HP-40 Nb alloy obtained by light microscopy (LM) after 0.5 h and 2h of ageing treatments performed at 1173K are given in Fig. 3a) and Fig. 3b), respectively. After short–term heat treatment (0.5h) at 1173K, the very fine precipitates of secondary carbides were found in the austenitic matrix, in zones close to primary carbides (Fig. 3a). The number of secondary carbide particles increases with ageing time (2 hours), as shown in Figure 3b. From Figure 3b it can be noticed clearly, that more fine secondary carbide particles precipitated in the matrix and agglomerated along the grain boundaries. Results of the EDS analysis of phases in the aged specimen at 1173K for 2h observed at SEM micrograph in Figure 4, are given in Table 3. The microstructure consists of an austenitic matrix (Spec.1) and two types of precipitates: one rich in Nb (white phase) - Spec.4, and one rich in Cr (dark gray phase) - Spec. 2, 3.

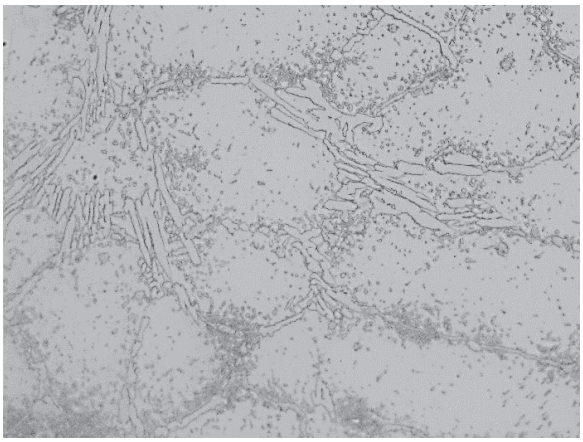

a) 500×

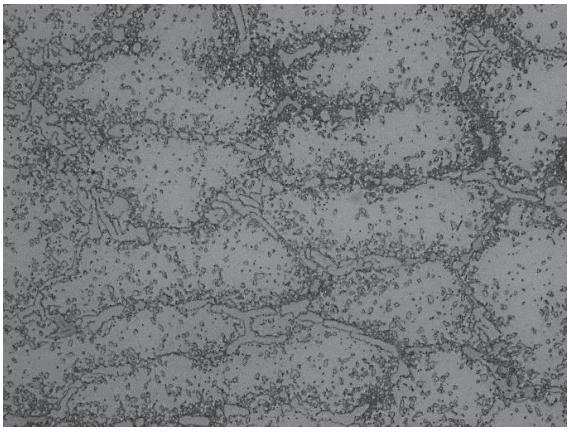

b) 500×

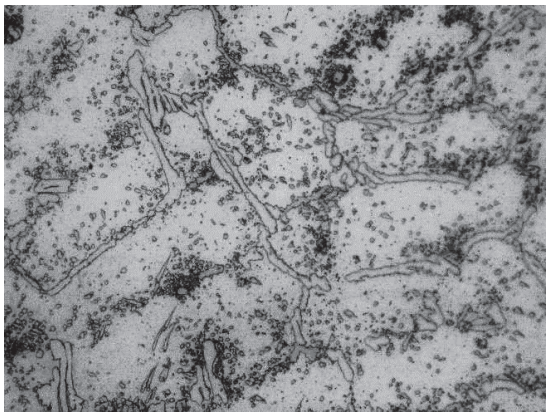

c) 500×

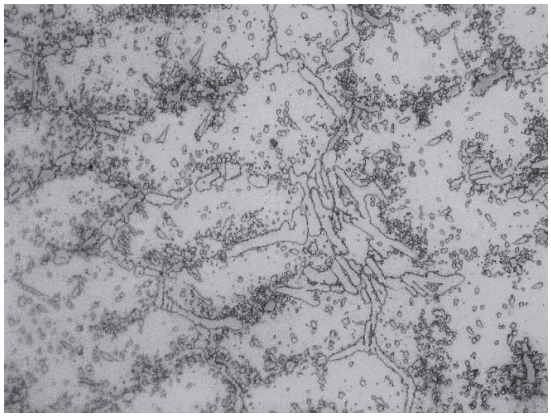

d) 500×

Figure 3: Light microscopy micrographs of a samples aged at: a) 1173K for 0.5h; 1173K for 2h; c) 1323K for 0.5h; d) 1323K for 2h

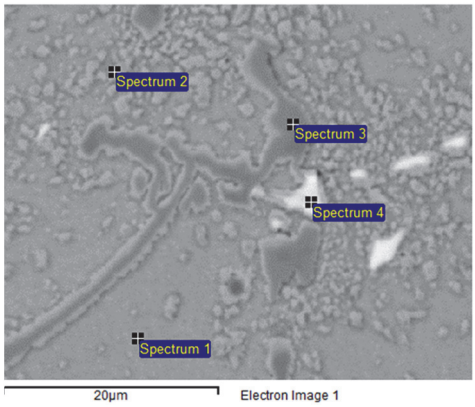

a)

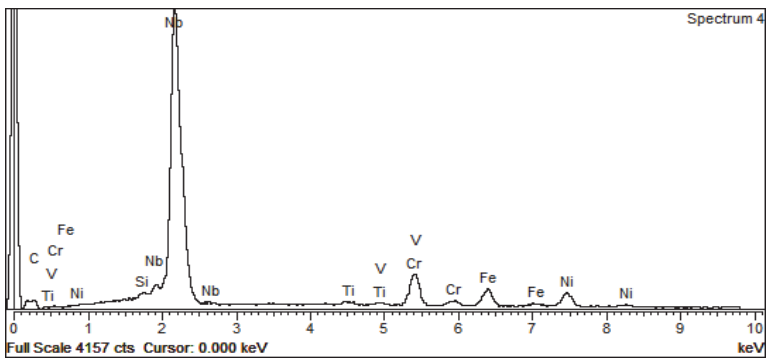

b)

Figure 4 Micrograph of present phases in 1173K aged HP40 Nb alloy: a) SEM micrographs (BSE), b) EDS spectrum of MC carbide (M= Nb) in examination point 4 (Spectrum 4)

Table 3: Chemical composition (mass%) of participate phases in HP40 Nb alloy, corresponding to Fig.4a

Spectrum	C	O	Si	Ti	V	Cr	Mn	Fe	Ni	Nb
Spectrum 1	4.12	0.89	1.25	-	-	21.22	1.32	36.35	34.85	
Spectrum 2	5.71		1.95			23.85	1.62	32.70	34.18	
Spectrum 3	7.69				0.51	75.96	2.06	10.47	3.31	
Spectrum 4	15.41		0.46	0.61	0.43	8.55		5.81	6.56	62.18

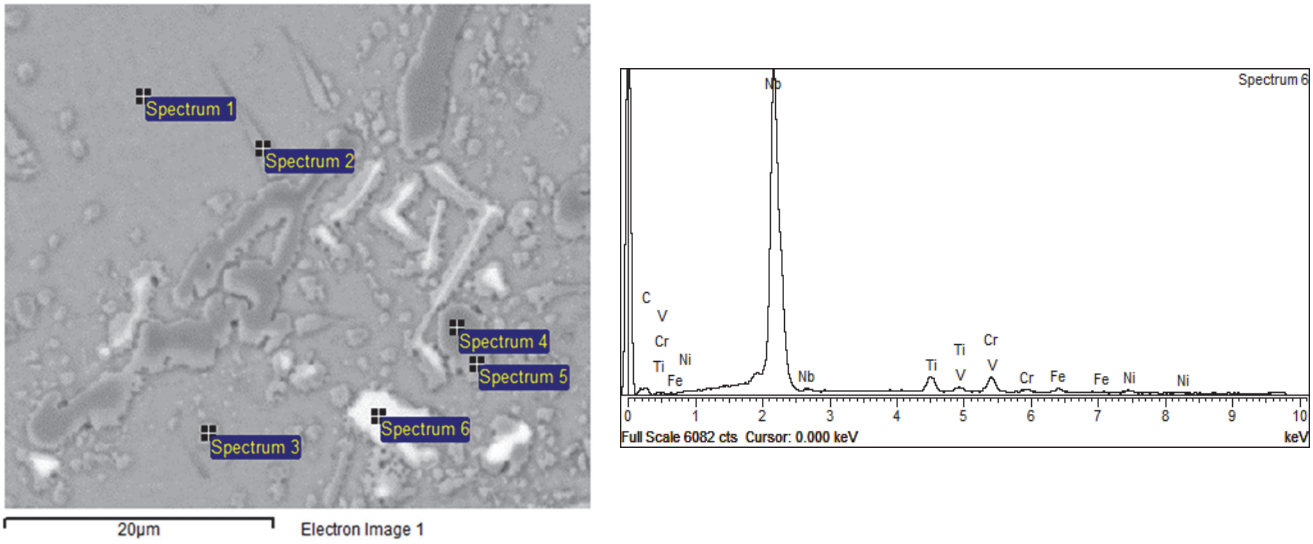

a) b)

Figure 5 Micrograph of present phases in 1323K aged HP40 Nb alloy: a) SEM micrographs (BSE), b) EDS spectrum in examination point 6 (Spectrum 6)

Table 4: Chemical composition (weight %) of participate phases in HP40 Nb alloy, corresponding to Fig.5a

Spectrum	C	Si	Ti	V	Cr	Mn	Fe	Ni	Nb
Spectrum 1	4.47	1.43			21.56	1.44	36.41	34.68	
Spectrum 2	6.33	1.41			26.91	1.45	32.02	31.88	
Spectrum 3	5.81	1.56			26.84	1.65	31.84	32.30	
Spectrum 4	9.16				70.38	1.81	12.61	5.59	0.45
Spectrum 5	6.55	1.46			27.85	1.64	30.82	31.67	
Spectrum 6	15.70		3.69	0.64	4.33		1.50	1.32	72.82

From Figure 5, it should be noted that the primary chromium carbides transform from M_7C_3 to $M_{23}C_6$. The secondary carbides were observed within the austenitic matrix close to the primary carbides. In this case, the microstructures after aging at 1323K for various aging times, are quite similar to those aged at 1173K, as can be seen in Fig.3c-d. However, it should be noted that the amount of needle-shaped $M_{23}C_6$ (M = Cr) type carbides formed in the austenitic matrix and secondary carbide film increased at this ageing condition [19].

3.5. Change of hardness during ageing

The Vickers hardness values determinations for samples aged at 1123K and 1323K and at different times are presented in Table 5. As can be seen, the different behavior in the evolution of the hardness for two temperatures of 1123K and 1323K. The hardness results after the lower temperature ageing are less than those of higher ones. The samples that have a maximum (207 HV10) and minimum hardness (197 HV10) were compared in their microstructures; for example, samples aged between 0.5h and 2 hours. The reason for this behavior can be explained by the change in the precipitate morphology and increased amounts of precipitates in the matrix.

Table 5: The results of Vickers hardness tests HV10 of the aged samples

Ageing temperature (K)	Ageing time (hours)	
	0.5	2
1123	197	207
1323	200	204

4. CONCLUSIONS

In this study, the microstructural evolution occurring in the HP 40 Nb heat-resistant stainless steel tube during the ageing was investigated. The obtained conclusions can be summarized as follows:

- After a short time of ageing (0.5h) at 1173K, the very fine precipitates of secondary carbides were found in the austenitic matrix, in zones close to primary carbides.
- The amount of the secondary carbide particles increases with ageing time (2 hours) at 1173K and more fine secondary carbide particles precipitated in the matrix and agglomerated along the grain boundaries.
- The microstructures after ageing at 1323K for various ageing times, are quite similar to those aged at 1173K. However, it should be noted that the amount of needle-shaped M23C6 (M = Cr) type carbides formed in the austenitic matrix and secondary carbide film increased at this ageing condition.
- The presence of these secondary carbides and change in the precipitate morphology in heat-treated specimens, resulting in higher values of hardness.

ACKNOWLEDGEMENTS

This work is supported by the Serbian Ministry for Education, Science and Technological Development by contracts No. 451-03-68/2022-14/200108, 451-03-68/2022-16/200156, No. 451-03-68/2022-14/200213.

REFERENCES

[1] D.J. Tillack and J.E. Guthrie, "Wrought and Cast Heat-Resistant Stainless Steels and Nickel Alloys for the Refining and Petrochemical Industries", Nickel Development Institute, Technical Series No. 10071, (1998)

[2] D.B. Roach and J.A. Van Echo, "Comparison of the Properties of the HK-40 and HP-45 Cast Heat-Resistant Alloys. Stainless Steel Castings, ASTM STP, Vol. 756, pp. 275-312. http://dx.doi.org/10.1520/STP28447S, (1982)

[3] W.T. Hou and R.W.K. Honeycombe, "Structure of Centrifugally Cast Austenitic Stainless Steels: Part 1 HK 40 as Cast and after Creep between 750˚C and 1000˚C", Materials Science and Technology, Vol. 1, pp. 385-389. http://dx.doi.org/10.1179/mst.1985.1.5.385, (1985)

[4] R.A.P. Ibañez, L.H. de Almeida, and I. Le May, "Effects of Si Content on the Microstructure of Modified-HP Austenitic Steels", Materials Characterization, Vol. 30, pp. 243-249. http://dx.doi.org/10.1016/1044-5803(93)90071-3, (1993)

[5] Blair, M.C. "Cast Stainless Steels", Metals Handbook, 1, ASM (USA), (1982)

[6] J. Rodríguez, S. Haro, A. Velasco, and R. Colás, "A Metallographic Study of Aging in Cast-Heat Resisting Alloy", Materials Characterization, Vol. 45, pp. 25-32, http://dx.doi.org/10.1016/S1044-5803(00)00047-4, (2000)

[7] L.H. de Almeida, A. F. Ribeiro, and I. Le May, "Microstructural Characterization of Modified 25Cr-35Ni Centrifugally Cast Steel Furnace Tubes", Materials Characterization, Vol. 49, pp. 219-229, http://dx.doi.org/10.1016/S1044-5803(03)00013-5, (2003)

[8] R. Voicu, E. Andrieu, D. Poquillon, J. Furtado and J. Lacaze, "Microstructure Evolution of HP40-Nb Alloys during Aging Under Air at 1000˚C", Materials Characterization, Vol. 60, pp. 1020-1027, https://doi.org/10.1016/j.matchar.2009.04.007, (2009)

[9] C.J. Liu and Y. Chen, "Variations of the microstructure and mechanical properties of HP40Nb hydrogen reformer tube with time at elevated temperature", Materials & Design, Vol. 32, pp. 2507–2512, https://doi.org/10.1016/j.matchar.2008.02.001, (2011)

[10] T. Dessolier, T. McAuliffe, W. J. Hamer, C. G.M. Hermse and T. B. Britton, "Effect of high temperature service on the complex through-wall microstructure of centrifugally cast HP40 reformer tube", Materials Characterization, Vol.177, p. 111070, https://doi.org/10.1016/j.matchar.2021.111070, (2021)

[11] C-M. Fuyang, J-Y. Chen, B. Shao, Y. Zhou, J-M.Gong, X-F. Guo and Y. Jiang, "Effect of microstructural evolution in thermal exposure on mechanical properties of HP40Nb alloy", International Journal of Pressure Vessels and Piping, International Journal of Pressure Vessels and Piping, Vol.192, p. 104391, https://doi.org/10.1016/j.ijpvp.2021.104391, (2021)

[12] A.F. Padilha, I.F. Machado, and R.L. Plaut, "Microstructures and Mechanical Properties of Fe-15%Cr-15%Ni Austenitic Stainless Steels Containing Different Level of Niobium Addition Submitted to Various Processing Stages", J. Mater. Process. Technol., Vol.170, pp. 89–96, https://doi.org/10.1016/j.jmatprotec.2005.05.002 , (2005)

[13] J.Laigo, F.Tancret, R. Le Gall and J. Furtado, "EBSD phase identification and modeling of precipitate formation in HP alloys", Vol. 15-17, pp. 702-707, Advance Materials Research, https://doi.org/10.4028/www.scientific.net/AMR.15-17.702, (2007)

[14] I. A. Sustaita –Torres, S. Haro-Rodríguez , M. P. Guerrero-Mata, M. de la Garza, E. Valdés, F. Deschaux-Beaume and R. Colás, "Aging of a cast 35Cr–45Ni heat resistant alloy", Materials Chemistry and Physics, Vol. 133, pp. 1018-1023, https://doi.org/10.1016/j.matchemphys.2012.02.010, (2012)

[15] A. Carlos Picasso, C. Armando L. Matías S. Lissarrague, A. Daniel Garófoli, "Microstructure Evolution of a Nickel-Base Alloy Resistant to High Temperature during Aging", Journal of Minerals and Materials Characterization and Engineering, Vol.4, pp.48-61 (2016), http://dx.doi.org/10.4236/jmmce.2016.41006

[16] I. Le May, T.L. Silveira and C.H. Vianna, "Criteria for the evaluation of damage and remaining life in reformer furnace tubes", Int. J.Press. Vessels Pip. Vol. 66, pp. 233-241, https://doi.org/10.1016/0308-0161(95)00098-4, (1996)

[17] G.D. De Almeida Soares, L.H. De Almeida, T.L. Da Silveira and I. Le May, "Niobium additions in HP heat-resistant cast stainless steels", Mater Characterization, Vol. 29, pp. 387–396, https://doi.org/10.1016/1044-5803(92)90045-J, (1992)

[18] J. Laigo F. Christien, R. Le Gall, F. Tancret and J. Furtado, "SEM, EDS, EPMA-WDS and EBSD characterization of carbides in HP type heat resistant alloys", Materials characterization, Vol.59, pp. 1580-1586, https://doi.org/10.1016/j.matchar.2008.02.001, (2008)

[19] T. Sourmail, "Precipitation in creep resistant austenitic stainless steels", Mater Sci Technol, Vol. 17, pp. 1–14, https://doi.org/10.1179/026708301101508972, (2001)

Engineering
TODAY
VOL. 1 / NO. 3 / 2022

CONTENTS